



HAL
open science

Dynamic mechanical response of ZrCu-based bulk metallic glasses

K. Tao, J. C. Qiao, L. Zhang, J. M. Pelletier

► **To cite this version:**

K. Tao, J. C. Qiao, L. Zhang, J. M. Pelletier. Dynamic mechanical response of ZrCu-based bulk metallic glasses. *International Journal of Mechanical Sciences*, 2021, 211, 10.1016/j.ijmecsci.2021.106770 . hal-03483005

HAL Id: hal-03483005

<https://hal.science/hal-03483005v1>

Submitted on 16 Oct 2023

HAL is a multi-disciplinary open access archive for the deposit and dissemination of scientific research documents, whether they are published or not. The documents may come from teaching and research institutions in France or abroad, or from public or private research centers.

L'archive ouverte pluridisciplinaire **HAL**, est destinée au dépôt et à la diffusion de documents scientifiques de niveau recherche, publiés ou non, émanant des établissements d'enseignement et de recherche français ou étrangers, des laboratoires publics ou privés.



Distributed under a Creative Commons Attribution - NonCommercial 4.0 International License

1 **Dynamic mechanical response of ZrCu-based bulk metallic**
2 **glasses**

3 K. Tao ^a, J.C. Qiao ^{a,b,*}, L. Zhang ^c, J.M. Pelletier ^{d,*}

4 ^a *School of Mechanics, Civil Engineering and Architecture, Northwestern*
5 *Polytechnical University, Xi'an 710072, China*

6 ^b *Chongqing Science and Technology Innovation Center of NPU, Chongqing 401135,*
7 *China*

8 ^c *Shi-changxu Innovation Center for Advanced Materials, Institute of Metal Research,*
9 *Chinese Academy of Sciences, Shenyang 110016, China*

10 ^d *Université de Lyon, MATEIS, UMR CNRS5510, Bat. B. Pascal, INSA-Lyon, F-69621*
11 *Villeurbanne Cedex, France*

12 * Corresponding author:

13 E-mail address: qjczy@nwpu.edu.cn (Professor Dr. J.C. Qiao)

14 jean-marc.pelletier@insa-lyon.fr (Professor Dr. J.M. Pelletier)

15

16 Abstract

17 The thermal stability and the dynamic mechanical relaxation behavior of
18 $(\text{Zr}_{50}\text{Cu}_{40}\text{Al}_{10})_{100-x}\text{Dy}_x$ (at.%) ($x=0$ or 2) metallic glasses were investigated by
19 differential scanning calorimetry (DSC) and dynamic mechanical analysis (DMA). In
20 the case of the $(\text{Zr}_{50}\text{Cu}_{40}\text{Al}_{10})_{100-x}\text{Dy}_x$ ($x=0$ or 2) metallic glasses, atomic mobility
21 increases by introduction of the Dy element. The activation energy of the the main α
22 relaxation process and fragility index were discussed according to the DMA
23 measurements. With the help of the time-temperature superposition (TTS) principle,
24 the master curves of the model alloys were established, the
25 Kohlrausch-Williams-Watts (KWW) function and quasi-point defects (QPD) theory
26 were used to describe the master curves of the metallic glasses. The characteristic
27 parameters related to microstructural heterogeneity in the KWW equation and the
28 QPD model, Kohlrausch exponent β_{KWW} and the correlation factor χ were
29 evaluated. In parallel, the elastic, viscoelastic and viscoplastic responses of the model
30 alloys have been analyzed based on the DMA results. Our investigations demonstrated
31 that introduction of the Dy increases the structure heterogeneity of the
32 $(\text{Zr}_{50}\text{Cu}_{40}\text{Al}_{10})_{100-x}\text{Dy}_x$ ($x=0$ or 2) glassy system, which plays an important role in
33 tailoring the dynamic relaxation behavior and mechanical properties of the metallic
34 glasses.

35 **Keywords:** Metallic glass; Mechanical relaxation process; Microstructure
36 heterogeneity; Quasi-point theory; Physical aging

37 1. Introduction

38 As a new class of metallic materials, metallic glasses (MGs) are well accepted to
39 have potential for wide application as engineering and functional materials due to
40 their unique physical/mechanical properties, such as the high strength and large elastic
41 limit [1-8]. The physical properties of MGs strongly depending on its internal
42 structural state at atomic level. It is well accepted that the metallic glasses are often
43 stay in out of equilibrium (more disorderly) and always evolve very slowly to a more
44 equilibrium state (more orderly) at ambient temperature in a rugged and tortuous

45 energy landscape due to the random long range atomic structure [9-11]. Compared
46 with the traditional metallic alloys, metallic glasses are absence of defects in metals,
47 i.e. voids, dislocations as well as grain boundaries. How to establish the correlation
48 between the “defects” and mechanical/physical properties is one of challenging issues
49 of metallic glasses [12, 13]. Many experiments and simulations have demonstrated
50 that metallic glasses are heterogeneous structure at micro-nano scale regions [2,
51 14-16]. Typically, the microstructure of the metallic glasses can be regarded as
52 liquid-like region and solid-like region [17-19]. Mechanical and physical properties of
53 metallic glass were inherited from the supercooled glass-forming liquid. Especially, it
54 is well documented that dynamic mechanical relaxation behavior is a key topic to
55 understand the the structural heterogeneity of metallic glasses [20, 21].

56 Dynamic mechanical analysis (DMA) (also called mechanical spectroscopy) is an
57 powerful technique to obtain the informations on the atomic or molecular movements
58 of glassy materials during the deformation process under a sinusoidal stress [22, 23].
59 According to the amplitudes of the stress, strain and phase lag, one can obtain some
60 fundamental parameters, such as storage modulus, loss modulus and internal friction
61 factor, et al. [24-26]. Benefitting from the advantages, DMA was widely used to probe
62 the α and β relaxation processes of the galssy solids. Importantly, as proposed by
63 Johari and Goldstein, the dynamic behaviour of metallic glasses is characterized by
64 two phenomenons: (i) JG relaxation or β relaxation process, which is linked to the
65 local movement of the atoms/molecules. The β relaxiaton is areversible process, and
66 (ii) the mian α relaxation, which is related to large scale irreversible arrangement of
67 atoms or molecules [27]. The dynamic relaxation modes provide an important route to
68 probe “defects” and to understand the corresponding the relation between structure
69 and property of metallic glass [12, 13]. Additionally, the glass main α relaxation
70 process corresponds to the dynamic glass transition phenomenon [5, 28]. It should be
71 stressed that β relaxation process is the main relaxation mode of the glassy solids.
72 [29]. It has been proposed that the β relaxation should be explained by the
73 translational motion of atoms localized in loosely packed regions. This description
74 certainly assumes that β relaxation intrinsically correlates with and structurally

75 originates from structural heterogeneity of metallic glasses [18, 19, 30].
76 Potential energy landscape (PEL) theory proposed by Debenedetti and Stillinger,
77 the β relaxation behavior has been interpreted as stochastically activated hopping
78 events through “subbasins”, while the α relaxation corresponds to the irreversible
79 hopping across various landscape megabasins [31]. As initially proposed by Argon
80 the deformation of MGs results from the cooperative shear motion of local
81 arrangements involving tens of hundred atoms, namely shear transformation zones
82 (STZs) [32, 33]. In addition, it has been observed that the activation energy of the β
83 relaxation is nearly the same as the potential energy barriers of STZs [34]. Therefore,
84 the dynamic relaxation behavior is intrinsic linked to the deformation mechanism of
85 glassy solids. Johnson and Samwer proposed that isolated events of the STZs
86 confined within the elastic matrix are linked to the β relaxation process, while
87 percolation of these STZs leads to the collapse of the confining matrix and breakdown
88 of elasticity are associated with the α relaxation [10, 35]. Therefore, understanding of
89 dynamic relaxation behavior is important issue for probing the nature of metallic glass,
90 microscopic structural heterogeneity, physical aging, deformation mechanism and the
91 mechanical properties. It is well known that physical properties of these dynamic
92 relaxation modes depend on the chemical composition of the metallic glasses.
93 According to previous researches, micro-alloying is an effective way to tune the
94 mechanical behavior and relaxation process [25, 36-40]. For instance, Yu et al.
95 reported that the intensity of β relaxation is suppressed by the introduction of
96 aluminum in a $\text{Cu}_{45}\text{Zr}_{45}\text{Al}_{10}$ metallic glasses [29]. The relaxation behavior of
97 ZrCu-based metallic glasses can also be modified by introducing hydrogen: α and β
98 relaxation shift to higher temperature region with a lower intensity, and a β'
99 relaxation occurs with relative higher intensity [38]. These samples with minor
100 addition of hydrogen element exhibit a higher density of “soft spots” , which
101 promotes the nucleation and occurrence of multiple shear bands. As a consequence,
102 plasticity of the metallic glasses could be ameliorated. It is widely known that “soft
103 spots” of the metallic glasses correspond to the loose-packed zones, which are easily
104 to initiate local arrangements. Previous literatures have pointed out that β relaxation

105 process is connected with these loose-packed zones [2, 41, 42]. Furthermore, it has
106 been demonstrated that by the addition of Dysprosium (Dy) of $(Zr_{50}Cu_{40}Al_{10})_{98}Dy_2$
107 glassy system, the β relaxation process becomes more evident and the compressive
108 plasticity is enhanced to some extent, which is ascribed to the improvement of
109 concentration of the “defects” of metallic glasses [25].

110 Many theoretical models have been developed to probe the deformation
111 mechanism and physical properties of amorphous materials i.e. free volume theory
112 [43-45], flow units model [46, 47] as well as interstitialcy theory [48, 49]. Free
113 volume is defined as the excess volume compared to an ideal disordered atomic
114 configuration of maximum density. Different from the free volume model, the
115 interstitialcy theory was originally proposed by Granato [48, 49]. It is widely accepted
116 that interstitials reside in a split configuration and sharing a lattice site with another
117 atom. In addition, flow units can be regarded as nanoscale regions which correspond
118 to pseudo “defects” in metallic glasses [21, 47]. Unlike the elastic matrix, the
119 nanoscale flow units show lower elastic moduli, higher energy state and lower
120 hardness. In parallel, Perez et al. assumed that the glass structure consists of packed
121 atoms with regions of enthalpy or entropy fluctuations [50-52]. These regions are
122 called quasi point defects (QPD). Compared to the crystals, a lower density region can
123 be seen as a vacancy, while a higher density region is comparable to an interstitial. The
124 QPD determine the atomic or molecular mobility through hierarchically correlated
125 atoms arrangements. The QPD theory refers to a conceptual scenario for the atomic
126 rearrangements occurring in favoured sites (defects) that are rich of free volume and
127 responsible for the non-elastic deformation. These movements can be dissociated in
128 anelastic (reversible) and viscoplastic (permanent) contribution [53]. Focusing on the
129 oxide glass and amorphous polymers, tremendous researches have been devoted to
130 the non-linear mechanical response to mechanical loading [22, 53, 54]. In principle,
131 their non-linear mechanical response is associated with the processes characterized by
132 a strong dependence on the temperature, strain rate and the intrinsic internal
133 heterogeneous atomic structure [19, 22, 54]. Therefore, modelling approaches are
134 needed to describe the feature behavior in order to allow us to predict or design the

135 function of metallic glass under the current circumstance of poor plasticity.

136 Micro-alloying is an important way to tune the mechanical properties of the
137 metallic glasses [25, 38, 39]. Furthermore, it has been demonstrated that by the
138 addition of dysprosium (Dy) of $\text{Cu}_{46}\text{Zr}_{43}\text{Al}_7\text{Dy}_4$ glassy system, the β relaxation
139 process becomes more evident and the compressive plasticity was enhanced to some
140 extent, which is ascribed to the improvement of concentration of the “defects” of
141 metallic glasses [25]. In the present study, the dynamic mechanical relaxation
142 processes of $(\text{Zr}_{50}\text{Cu}_{40}\text{Al}_{10})_{100-x}\text{Dy}_x$ ($x=0$ or 2) metallic glasses were investigated by
143 DMA. In the framework of the QPD theory, dynamic mechanical behavior of the
144 model alloys were described. The experimental results suggested that introduction of
145 the Dy increases the structure heterogeneity of the $(\text{Zr}_{50}\text{Cu}_{40}\text{Al}_{10})_{100-x}\text{Dy}_x$ ($x=0$ or 2)
146 metallic glasses. It should be emphasized that micro-alloying is an important
147 technique to tailor the dynamic relaxation modes of metallic glasses.

148 **2. Experiment procedure**

149 The samples with nominal composition $(\text{Zr}_{50}\text{Cu}_{40}\text{Al}_{10})_{100-x}\text{Dy}_x$ ($x=0$ or 2) were
150 prepared by the arc-melting technique. Master-alloy ingots were first prepared using a
151 mixture of high purity (99.99%) Zr, Cu, Al and Dy elements in an argon atmosphere.
152 The master alloy was re-melted at least five times to ensure the chemical
153 homogeneity of the model alloys. Metallic glass plates with a thickness of 2 mm
154 were prepared by copper mould casting technique.

155 X-ray diffraction (XRD) was conducted to confirm the glassy nature by $\text{Cu K}\alpha$
156 radiation produced by a Bruker D8 advance X-ray diffractometer at room temperature.
157 The specimens were checked by Transmission electron microscopy (TEM, FEI Titan
158 G3) with probe and image Cs correctors. TEM specimens were cut from the samples
159 and ion milled using a Gatan 695 device. Differential scanning calorimetry (DSC)
160 experiments were performed through a commercial instrument (DSC, PerkinElmer) at
161 a heating rate of 10 K/min in a high purity dry nitrogen atmosphere. The glass
162 transition temperature and the onset crystallization temperature were determined
163 based on the DSC curve.

164 Plate samples were cut with approximate dimensions 30 (length) \times 2.0 (width) \times
165 1.0 mm (thickness) by an electric discharge machine, then polished by 2000 grit SiC
166 paper. Finally, the samples were sonicated in a methanol bath to remove surface
167 contaminants. The dynamic relaxation behavior of metallic glasses was investigated
168 using two different DMA devices, i.e. a commercial device (DMA, Q800, TA, USA)
169 and a home-made inverted torsion instrument with a vacuum environment in INSA de
170 Lyon [55]. The first one uses tensile stress, leading to the determination of the Young
171 modulus (E), while in the second one a shear stress is applied and the shear modulus
172 (G) is deduced. A periodic stress is applied $\sigma = \sigma_0 \sin(\omega t)$, where ω is the angular
173 frequency. The complex modulus E^* , which can be defined as $E' + iE''$, and shear
174 modulus, $G^* = G' + iG''$, can be deduced from σ/ε , where E' and G' are the
175 storage modulus, E'' and G'' are the loss modulus. Consequently, the loss factor,
176 also termed as internal friction, $\tan \delta = E''/E'$ or $\tan \delta = G''/G'$ can be determined.
177 It should be noted here that $\tan \delta$ is related to the energy loss per load cycle:
178 $\tan \delta = 1/2\pi(\Delta W/W)$, where the energy loss ΔW is caused by the movement of
179 atoms during relaxation process. Two different kinds of experiments were performed:
180 (i) Isochronal tests were conducted with a single cantilever mode at a heating rate of 3
181 K/min and a driving frequency of 1 Hz on the DMA Q800. (ii) Isothermal
182 experiments were carried on the home-made inverted torsion instrument with various
183 frequency from 0.01 to 2 Hz (the temperature interval is 5 K).

184 **3. Experimental results and discussions**

185 ***3.1 Structural and thermal properties of the $(Zr_{50}Cu_{40}Al_{10})_{100-x}Dy_x$ ($x=0$ or 2)*** 186 ***metallic glasses***

187 XRD were performed to check the amorphous nature of the
188 $(Zr_{50}Cu_{40}Al_{10})_{100-x}Dy_x$ ($x=0$ or 2) (as-cast state) metallic glasses. As shown in **Fig.1**
189 **(a)**, the XRD patterns exhibit a broad maximum with no detectable crystalline Bragg
190 peaks, which suggests that the model alloys are fully amorphous.

191 The glass transition and crystallization events were determined by DSC, which is
192 shown in **Fig.1 (b)**. In the case of the $Zr_{50}Cu_{40}Al_{10}$ and $(Zr_{50}Cu_{40}Al_{10})_{98}Dy_2$ bulk

193 metallic glasses, the glass transition temperature T_g is 691 K and 683 K, respectively.
194 At the same time, the crystallization temperature of $Zr_{50}Cu_{40}Al_{10}$ and
195 $(Zr_{50}Cu_{40}Al_{10})_{98}Dy_2$ is 763 K and 756 K, respectively. It is evident that T_g is
196 decreased by the addition of Dy. In parallel, in good agreement with other Zr-based
197 metallic glasses, the $(Zr_{50}Cu_{40}Al_{10})_{100-x}Dy_x$ ($x=0$ or 2) bulk metallic glasses show
198 broad super-cooled liquid regions (SLRs) [24, 25]. In addition, as shown in **Fig.2**, the
199 glassy structure was confirmed by the featureless TEM microstructures and the
200 high-resolution TEM (HRTEM) images, of which the corresponding fast Fourier
201 transformation (FFT) patterns only present a diffuse halo, further confirming that the
202 amorphous structure of the model alloys in the current investigations. It should be
203 emphasized that there is no formation of oxide inclusions in the introduction of the
204 rare earth metals of $(Zr_{50}Cu_{40}Al_{10})_{100-x}Dy_x$ ($x=0$ or 2) bulk metallic glasses.

205 **3.2 Dynamic mechanical analysis**

206 **3.2.1 Isochronal analysis**

207 In order to probe the dynamic mechanical behavior of the $(Zr_{50}Cu_{40}Al_{10})_{100-x}Dy_x$
208 ($x=0$ or 2) metallic glasses, the samples were heated in the isochronal mode by DMA.
209 **Fig.3 (a)** shows the normalized storage modulus E'/E_u and the normalized loss
210 modulus E''/E_u of $(Zr_{50}Cu_{40}Al_{10})_{98}Dy_2$ metallic glass. Herein, it should be stressed
211 that E_u is the unrelaxed modulus at the room temperature, which is assumed as the
212 value of the storage modulus at ambient temperature. Evidently, compared with the
213 storage modulus, the contribution of loss modulus during the deformation process at
214 the ambient temperature could be neglected. There are three temperature regions can
215 be observed based on the temperature-heating process of the model alloy (as shown in
216 **Fig.3 (a)**), which is similar to other typical metallic glasses [25, 56]. (I) When the
217 temperature below 630 K, the normalized storage modulus E' is high and nearly
218 remains constant, while the normalized loss modulus around zero. It suggests that the
219 elastic deformation dominates the deformation process in this temperature domain. As
220 we mentioned in the Introduction section, unlike the La-based metallic glasses [26],
221 there is no pronounced β relaxation peak was observed of the ZrCu-based metallic

222 glass. (II) When the temperature ranges from 630 K to 740 K, it can be seen that
223 the storage modulus E' decreases drastically. On the other hand, the loss modulus
224 E'' increases, which reaches the maximum value around 725 K, which corresponds to
225 the α relaxation of glassy materials. Generally speaking, the α relaxation process of
226 glasses, which is closely associated with the cooperative movements of the atoms
227 or molecules [23, 25]. (III) When the temperature above 740 K, it is found that the
228 storage modulus E' and the loss modulus E'' increase sharply, which corresponds
229 to the precipitation of the crystalline phases.

230 In parallel, dynamic mechanical relaxation processes of metallic glasses is very
231 sensitive to the driving frequency. **Fig.3 (b)** shows the normalized loss modulus of
232 $(\text{Zr}_{50}\text{Cu}_{40}\text{Al}_{10})_{98}\text{Dy}_2$ metallic glass *versus* the temperature at different frequencies (1,
233 2, 4 and 8 Hz) with a constant heating rate of 3 K/min. The α relaxation peak shifts to
234 a higher temperature by increasing the driving frequency. The activation energy can
235 be deduced from the correlation between the driving frequency and the characteristic
236 temperature by the Arrhenius equation [52]:

$$237 \quad f = f_0 \exp\left(-\frac{E_\alpha}{k_B T_p}\right) \quad (1)$$

238 where f is the driving frequency, f_0 is a pre-exponential factor, E_α is the
239 activation energy of the main α relaxation and T_α is the characteristic temperature of
240 α relaxation. As a consequence, the activation energy of the $\text{Zr}_{50}\text{Cu}_{40}\text{Al}_{10}$ and
241 $(\text{Zr}_{50}\text{Cu}_{40}\text{Al}_{10})_{98}\text{Dy}_2$ metallic glasses is 5.73 eV and 5.57 eV, respectively. The results
242 in the current research are in good agreement with the other typical ZrCu-based
243 metallic glasses [56, 57].

244 In the case of metallic glasses, the dynamic relaxation behavior is closely linked
245 to the fragility parameter [58]. Angell proposed the kinetic fragility m , which is
246 connected to the slow down of glass transition dynamics and proposed to characterize
247 the deviation from the Arrhenius relationship in the characteristic relaxation time
248 *versus* temperature curve [12, 59]. It is accepted that the concept of fragility has been
249 used to classify the viscosity or the relaxation time of glass forming liquid with
250 temperature approaching the glass transition temperature T_g , and can be defined by

251 [59, 60]:

$$252 \quad m = d \log_{10} \tau_{\alpha} / d(T_g/T) = E_{\alpha} / (RT_g \ln 10) \quad (2)$$

253 From the m value we can learn how fast the viscosity decreases near the glass
254 transition temperature T_g [59]. Typically, the fragility parameter m of the glassy
255 materials ranges from 16 to 200 [59]. In the current study, the fragility parameter m
256 is = 41 for $Zr_{50}Cu_{40}Al_{10}$ metallic glass. Compared with other metallic glasses, four
257 fragile metallic glass formers were chosen: $Zr_{41.2}Ti_{13.8}Cu_{12.5}Ni_{10}Be_{22.5}$ ($m=50$),
258 $La_{60}Ni_{15}Al_{25}$ ($m=51$), $Al_{88}Y_7Fe_5$ ($m=55$) and $Gd_{55}Co_{25}Al_{20}$ ($m=74$) [9]. It indicates that
259 the current ZrCu-based metallic glass is a stronger glassy system due to the value of
260 fragility parameter m is lower. We will discuss the information of fragility of glassy
261 solids in the next section. Therefore, following the criteria defined in the reference
262 [50], it is reasonable to believe that ZrCu-based metallic glasses have a dense-packed
263 structure and a high glass-forming ability.

264 The temperature dependence of the normalized loss modulus E''/E_u for the
265 $(Zr_{50}Cu_{40}Al_{10})_{100-x}Dy_x$ ($x=0$ or 2) metallic glasses is shown in **Fig.4**. The peak
266 temperature of the normalized loss modulus moves to the lower temperature by the
267 addition of Dy, which is in accordance with the results of glass transition temperature
268 obtained by DSC (which was shown in **Fig.1 (b)**).

269 It should be noted that the JG relaxation is not clearly observed at the low
270 temperature region [25, 40] (**Fig. 4**). However, there is only broad hump (sometimes
271 referred as excess wings) can be observed around 560-650 K and 575-660 K for
272 $Zr_{50}Cu_{40}Al_{10}$ and $(Zr_{50}Cu_{40}Al_{10})_{98}Dy_2$ bulk metallic glasses, respectively [58]. These
273 humps may be considered as large and diffuse JG relaxations (Excess wing). The
274 magnitude of the excess wing is increased by increasing the Dy content. The influence
275 of micro-alloying on the JG relaxation in the $(Zr_{50}Cu_{40}Al_{10})_{100-x}Dy_x$ ($x=0$ or 2) glassy
276 system needs to be addressed from a perspective of mixing enthalpy in metallic glass
277 systems. The JG relaxation is linked to dynamic heterogeneity in metallic glasses,
278 especially a local diffusion in loose-packed isolated regions which are often referred as
279 defects and flow units [9, 18, 23]. The mixing enthalpy of Zr-Cu, Zr-Al, Zr-Dy are

280 -23, -44 and 8 kJ/mol, while the mixing enthalpy of Cu-Al, Cu-Dy and Al-Dy are -1,
 281 -22 and -38 kJ/mol, respectively [61, 62]. According to the empirical rules to
 282 determine ΔH_{mix} , the mixing enthalpy of the $(Zr_{50}Cu_{40}Al_{10})_{100-x}Dy_x$ ($x=0$ or 2)
 283 metallic glasses is -30.88 ($x=0$) and -31.55 ($x=2$), respectively. Therefore, the addition
 284 of Dy decreases the mixing enthalpy, which explains the increase in the intensity of
 285 the β relaxation, or at least the value of the loss modulus at low temperature. Similar
 286 conclusions have been obtained in previous studies [25, 29]. In addition, the peak of
 287 the loss factor moves to lower temperature, which agrees with the phenomena
 288 observed on the DSC curve, moving to lower temperature in **Fig.1 (b)**.

289 Perez and his coworkers proposed the quasi-point defect theory, which can be
 290 used to describe the mechanical properties of amorphous materials with respect to its
 291 microstructure [51, 52, 63, 64]. The atomic rearrangement will preferentially occur at
 292 these defect sites, whether in the process of thermal activation or stress activation.
 293 **Fig.5 (a)** shows a symbolic scheme of an amorphous solids with the associated defect
 294 sites. The effect of a mechanical stimulus such as a shear stress is applied. At the first
 295 stage of the deformation, these sites are thermomechanical activated under the
 296 mechanical stimulus (as seen in **Fig.5 (b)**), which bring the localized elementary
 297 motions of several atoms or molecules, preferentially oriented along the maximum
 298 shear plane. It should be noted that these atomic rearrangements are responsible to the
 299 second β relaxation process of amorphous solids [29]. The nucleation and growth
 300 from these sheared micro domains are responsible to the onset of the inelastic
 301 response of the glassy materials (as shown in **Fig.5 (c)**). When the applied stress is
 302 long enough, new sheared micro domains are nucleated (as seen in **Fig.5 (d)**),
 303 which causes plastic deformation by the coalescence of shear micro domains. The
 304 dynamic relaxation behavior is generally related to atomic or molecular motions and
 305 the relaxation time is temperature dependence. As described in earlier reports [65, 66],
 306 the hierarchically correlation of dynamic relaxation leads to the following expression
 307 for the mean time τ_{mol} , which characterizes the atomic mobility as:

$$308 \quad \tau_{mol} = t_0 \left(\frac{\tau_{\beta}}{t_0} \right)^{1/\chi} \quad (3)$$

309 where τ_{mol} corresponds to the mean duration of the movement of a structural unit
 310 over distance equal to its dimension. τ_β is the mean time of the thermally activated
 311 jump of structural units and follows an Arrhenius law:

$$312 \quad \tau_\beta = \tau_{0\beta} \exp\left(\frac{U_\beta}{kT}\right) \quad (4)$$

313 where U_β is the apparent activation energy for the movements of structural units and
 314 is then related to the β relaxation mode of glassy solids. t_0 is a scaling factor and χ
 315 is a correlation factor range from 0 to 1:

316 (I) $\chi = 0$: any movement of a structural units requires the motion of all other
 317 units (maximum order, corresponding to a perfect crystal).

318 (II) $\chi = 1$: all the movements are independent on each other (maximum disorder,
 319 corresponding to a perfect gas). Should note that, **Eq.(4)** only express the thermal
 320 activation process, so it can be modified to characterize the mechanical activation
 321 [65]:

$$322 \quad \tau_\beta = \tau_{0\beta} \exp\left(\frac{(U_\beta + \Omega p)\left(1 - \frac{\sigma_{max}}{\sigma_0}\right)^{3/2}}{kT}\right) \quad (5)$$

323 where p is the hydrostatic pressure, Ω is the shear stress which enables the energy
 324 cross-over at 0 K. σ_{max} is the activation shear stress or the maximum shear stress.

325 Because the correlation parameters are connected to the disordered state, it is
 326 reasonable to be related to the microstructure evolution. If one neglects the aging
 327 effect and without any external stimulus, the disorder is assumed constant in a “frozen”
 328 glass state, whereas it increases linearly with temperature when the temperature rises
 329 to the glass transition temperature T_g . In addition, taking the scenario proposed for
 330 atoms rearrangements under an external mechanical stimulus, the disorder parameter
 331 must be related to the state of non-elastic strain within the sample. Besides, an
 332 increase of the anelastic component corresponds to an increase of the number/size
 333 of QPD, i.e., an increase of the disorder. However, the viscoplastic process may
 334 provoke the decrease of the disorder due to it leads to the larger scale atomic
 335 rearrangements. So, in a frozen or iso-configurational state, χ has a constant value,
 336 while in a metastable thermodynamic equilibrium, χ increases with the temperature

337 T . The variation of the correlation factor χ with the temperature can be expressed by
 338 [67]:

$$339 \quad \chi(T, \gamma) = \chi(T) + a_{ve}\gamma_{ve} - a_{vp}\gamma_{vp} \quad (6-1)$$

$$340 \quad \chi(T) = \chi(T_g), \quad T < T_g \quad (6-2)$$

$$341 \quad \chi(T) = \chi(T_g) + a(T - T_g), \quad T > T_g \quad (6-3)$$

342 where a_{ve} , a_{vp} and a depend on the material.

343 The atomic mobility is assisted by the microscopic structure heterogeneity in
 344 metallic glass, from the point of the potential energy landscape theory, i.e., nanoscale
 345 fluctuations of the entropy or enthalpy. These fluctuations can be described as
 346 quasi-point defects (QPD), Their concentration C_d is temperature dependence and
 347 can be evaluated from the Boltzmann statistics [51]:

$$348 \quad C_d = \left(1 + \exp\left(-\frac{\Delta S_F}{k}\right) \exp\left(\frac{\Delta H_F}{kT}\right) \right)^{-1} \quad (7)$$

349 where ΔS_F and ΔH_F is the function entropy and enthalpy of a QPD, respectively.

350 According to the concepts mentioned above, the compliance $J(t)$ is the
 351 combination of elastic, anelastic and viscoplastic components of the deformation. In
 352 amorphous solids, $J(t)$ can be described as [54]:

$$353 \quad J(t) = \frac{1}{G_{el}} + A \left\{ 1 - \exp\left[-\left(\frac{t}{\tau_{mol}}\right)^\chi\right] \right\} + A' \left(\frac{t}{\tau_{mol}}\right) \quad (8)$$

354 where G_{el} is the elastic modulus at infinite frequency, A and A' are parameters
 355 proportional to quasi-point concentration C_d , thus, also proportional to the anelastic
 356 component of the deformation. The description of the dynamic modulus and the
 357 frequency can be simply given by the Fourier transform of **Eq.8**, and considering the
 358 residual component of the modulus, i.e., $G_r = G(\infty)$:

$$359 \quad G^*(i\omega) = G_r + \frac{G_{el} - G_r}{1 + \eta(i\omega\tau_{mol})^{-\chi} + (i\omega\tau_{mol})^{-1}} \quad (9)$$

360 where G_u is the unrelaxed modulus, η is a numerical factor, near unity, but
 361 depending on C_d , ω is the angular frequency.

362 Furthermore, Perez et al. [64] have given the expression of the internal friction
 363 $\tan \delta = G''/G'$:

$$364 \quad \ln(\tan \delta) = \frac{U_\beta}{kT} - \chi \ln \omega - \chi \ln \tau^* + \ln \eta \quad (10)$$

365 with:

$$366 \quad \tau^* = t_0 \left(\frac{\tau_0 \beta}{t_0} \right)^{1/\chi} \quad (11)$$

367 When the temperature below the glass transition temperature T_g , the material is
368 in an iso-configurational state and χ is constant. On the other hand, when the
369 temperature above the glass transition temperature T_g the concentration of defect
370 increases due to a faster diffusion, and therefore χ increases. Consequently, one can
371 plots $\ln(\tan \delta)$ versus the reciprocal of the temperature $1/T$ at a fixed frequency
372 and then get the value of U_β . In a similar method, χ can be deduced from the plot of
373 $\ln(\tan \delta)$ versus $\ln(\omega)$ at a fixed temperature.

374 **Fig.6** shows the logarithm of internal friction $\ln(\tan \delta)$ versus the reciprocal of
375 the temperature $1/T$ for the $(\text{Zr}_{50}\text{Cu}_{40}\text{Al}_{10})_{100-x}\text{Dy}_x$ ($x=0$ or 2) bulk metallic glasses.
376 Such a plot can be used to determine the glass transition temperature T_g and
377 crystalline temperature T_x . In fact, the aforementioned theory has been successfully
378 used by previous researches to analyze viscoelasticity and viscoplasticity behavior in
379 Zr- and Pd-based bulk metallic glasses [68, 69]. The characteristic parameters for both
380 alloys obtained from mechanical spectroscopy analysis based upon the physical model
381 are summarized in the **Table 1**.

382 **Table1** The characteristic parameters determined by mechanical spectroscopy analysis

Metallic glasses	T_g (K)	T_x (K)	$T_x - T_g$ (K)	U_β (eV)
$\text{Zr}_{50}\text{Cu}_{40}\text{Al}_{10}$	693	752	59	0.628
$(\text{Zr}_{50}\text{Cu}_{40}\text{Al}_{10})_{98}\text{Dy}_2$	681	738	57	0.578

383 As shown in **Table 1**, glass transition temperature T_g , temperature corresponding
384 to the onset of crystallization T_x and the range of super-cooled liquid $\Delta T_x = T_x - T_g$
385 decrease with Dy element addition, which is consistent with the results of calorimetric
386 analysis. It should be noted that the values of the characteristic temperatures deduced
387 from the dynamic mechanical spectroscopy analysis are very close to that obtained
388 through the DSC curves. It can be clearly seen that the activation energy U_β , which is
389 the height of the energy barrier for the elementary movement related to the β

390 relaxation for the $Zr_{50}Cu_{40}Al_{10}$ and the $(Zr_{50}Cu_{40}Al_{10})_{98}Dy_2$ metallic glasses is 0.628
391 and 0.578 eV, respectively. The experimental results demonstrates that the addition of
392 Dy element enhances the atomic mobility, thus decreases the mean time τ_β and the
393 relaxation time of related β relaxation. Based on the cooperative shear model, the
394 activation energy E_β is equivalent to the potential energy barrier for operating of
395 STZs, a lower activation energy E_β linking to a compliant matrix confinement [10,
396 70, 71]. Besides, the β relaxation closely relates to the plasticity in metallic glass,
397 which is believed as a thermal-driven percolation process of STZs [34]. It is reported
398 that the STZs prefer to nucleating in the liquid like region [29, 72]. Thus, we can
399 assumed that the lower the activation energy, the more the STZs could be triggered.
400 This in turn will promote the nucleation and propagation of shear bands and
401 potentially improve the plasticity in metallic glasses [38].

402 **3.2.2 Physical aging of metallic glass**

403 Kinetics of the structural relaxation in $(Zr_{50}Cu_{40}Al_{10})_{98}Dy_2$ bulk metallic glass
404 was investigated by performing isothermal DMA measurements with a driving
405 frequency of 1 Hz. **Fig.7** (blue line) shows the loss factor $\tan \delta$ evolution *versus*
406 annealing time at 625 K in the $(Zr_{50}Cu_{40}Al_{10})_{98}Dy_2$ bulk metallic glass. The loss factor
407 $\tan \delta$ decreases sharply with the annealing time, while the storage modulus E'
408 increases slightly.

409 Dynamic mechanical relaxation process in amorphous materials presents
410 non-exponential, non-Arrhenius and nonlinear characteristics. It is believed that
411 physical aging below the glass transition temperature can tune the physical and
412 mechanical behaviors of glassy materials [24, 73, 74]. From the perspective of the
413 kinetics, the Kohlrausch-Williams-Watts (KWW) equation was widely used to
414 describe the kinetics of physical aging of amorphous materials based on DSC
415 experimental results as well as DMA experiments [12, 13, 56]. The KWW function is
416 defined as follows [75]:

$$417 \quad \tan \delta(t = 0) - \tan \delta(t) = A\{1 - \exp[-(t_a/\tau)^{\beta_{aging}}]\} \quad (12)$$

418 where $A = \tan \delta(t) - \tan \delta (t \rightarrow \infty)$ is the maximum magnitude of the relaxation.
419 t_a stands for the aging time, τ is characteristic relaxation time and β_{aging} is the
420 Kohlrausch exponent, which ranges from 0 to 1, which is related to the dynamic
421 inhomogeneity [47].

422 The solid lines in **Fig.6** represents the fitted curve using **Eq. (12)**. The
423 Kohlrausch exponent β_{aging} is around 0.50 when the physical aging temperature is
424 close to the glass transition temperature T_g of $(Zr_{50}Cu_{40}Al_{10})_{98}Dy_2$ metallic glass,
425 which is in accordance with previous reported experimental results [24].

426 The annealed sample has been reheated after the process of physical aging. The
427 inset of **Fig.8 (b)** shows the schematic illustration of the temperature history during
428 the *in-situ* heating process. As shown in **Fig.8 (a)**, the storage modulus of annealed
429 sample is higher than that of the as-cast state. But there is an interesting phenomenon
430 in **Fig.8 (b)**, an evident peak which is like the β relaxation process can be noticed in
431 the annealed metallic glasses [29, 40]. We speculate that it could be due to phase
432 separation during the physical aging process. However, a more detailed scrutinize is
433 required, and it will be reported in the other work. **Fig.9** is the HRTEM image of the
434 annealed sample of $(Zr_{50}Cu_{40}Al_{10})_{98}Dy_2$ metallic glass. It is evident that there is no
435 formation of nucleation or crystalline phase during the physical aging process of the
436 model alloy. As we discussed in the previous section, it should be noted that the
437 glassy materials are in a non-equilibrium state below the glass transition temperature
438 T_g . For metallic glasses or other amorphous materials, when the annealing
439 temperature T_a is below T_g , the structure of the glassy materials tends towards more
440 stable state [4]. As shown in **Fig.10**, the difference in specific heat capacity, Δc_p ,
441 induced by physical aging and as-cast state of $(Zr_{50}Cu_{40}Al_{10})_{98}Dy_2$ metallic glass. It
442 should be emphasized that the as-cast state shows a noticeable signal of relaxation
443 enthalpy $\Delta H = (1.61 \pm 0.06) \text{ kJ mol}^{-1}$ near T_g , which indicating that the specimen
444 has certain free volume content after suction mold casting. It is reported that the
445 sub- T_g physical aging of glassy materials is accompanied by reduction of free volume,
446 which is closely connected with topological short-range ordering and chemical

447 short-range ordering [76]. The decrease of the free volume is accompanied by a
 448 decrease of the enthalpy of the metallic glass. As a consequence, isothermal annealing
 449 below the glass transition temperature leads to a reduction of the free volume up to
 450 $\Delta H = (0.35 \pm 0.04) \text{ kJ mol}^{-1}$. Besides, noted that, an increase of the endothermic
 451 effect can be observed, which is ascribed to more free volume generation takes place
 452 in a relaxed specimen [76].

453 *3.2.3 Isothermal frequency scanning analysis*

454 In order to further study the dynamic mechanical relaxation behavior, isothermal
 455 frequency scanning experiments were carried out in the $(\text{Zr}_{50}\text{Cu}_{40}\text{Al}_{10})_{100-x}\text{Dy}_x$ ($x=0$ or
 456 2) metallic glasses (as shown in **Fig.11**). The experimental results could be
 457 summarized as follows: (i) At the lower frequency, the storage modulus G' is low. (ii)
 458 The loss modulus G'' shows a peak corresponding to the α relaxation at high
 459 temperature, and it shifts toward to a lower frequency when temperature decreases.
 460 (iii) There is no evident JG relaxation behavior according to the loss modulus.

461 From the prespective of the frequency window, the pronounced peaks
 462 wereobserved at high temperature, which corresponds to the main α relaxation of
 463 metallic glasses. This is in line with the results obtained in **Fig.3 (a)**. The
 464 characteristic time of the α relaxation τ_α of metallic glass can be obtained from the
 465 general relation: $2\pi f\tau_\alpha = 1$.

466 On the basis of the time-temperature superposition (TTS) principle, master curve
 467 may be plotted with a reference temperature. The initial curves are shifted by the
 468 frequency shift factor a_T [77, 78]:

$$469 \quad \ln a_T = \ln \tau - \ln \tau_r \quad (13)$$

470 where τ and τ_r are the relaxation times at temperatures T and the reference
 471 temperature T_r , respectively. The variation of the relaxation time τ with temperature
 472 may be described using the following equation [78]:

$$473 \quad \ln a_T = \frac{E_\alpha}{R} \left(\frac{1}{T} - \frac{1}{T_r} \right) \quad (14)$$

474 where R is the gas constant and E_α is the activation energy of the α relaxation.

475 **Fig.12** shows the master curves of $(\text{Zr}_{50}\text{Cu}_{40}\text{Al}_{10})_{100-x}\text{Dy}_x$ ($x=0$ or 2) metallic

476 glasses. As proposed by Williams et al., the Kohlrausch-Williams-Watts (KWW)
 477 relaxation relation can be used to well describe the α relaxation process of the loss
 478 modulus spectra of glassy solids [79]:

$$479 \quad G''(\omega) = \Delta G_\alpha L_{i\omega} \left[-\frac{d\varphi_\alpha(t, \tau_\alpha)}{dt} \right] \quad (15)$$

480 With:

$$481 \quad \varphi_\alpha(t, \tau_\alpha) = \exp\left[-(t/\tau_\alpha)^{\beta_{KWW}}\right] \quad (16)$$

482 where ΔG_α is the relaxation strength, which is equal to the difference between the
 483 unrelaxed modulus G_u and the well relaxed modulus G_r . $L_{i\omega}$ indicates the Laplace
 484 transform, and β_{KWW} stands for the Kohlrausch exponent, which ranges from 0 to 1
 485 and can be obtained from the isothermal spectra.

486 Based on the previous investigations, Bergman derived a relaxation equation,
 487 which can be used to the main relaxation process of the amorphous materials (i.e.
 488 metallic glasses as well as amorphous polymers) [80]:

$$489 \quad G'' = G_p / \left\{ 1 - \beta_{KWW} + \frac{\beta_{KWW}}{1 + \beta_{KWW}} \left[\beta_{KWW} (\omega_p / \omega) + (\omega / \omega_p)^{\beta_{KWW}} \right] \right\} \quad (17)$$

490 where G_p is the normalized loss modulus and ω_p indicates the peak frequency.

491 As shown in **Fig.12 (a)**, the master curves of $(Zr_{50}Cu_{40}Al_{10})_{100-x}Dy_x$ ($x=0$ or 2)
 492 metallic glasses can be well described by **Eq.(17)**. The value of β_{KWW} in
 493 $Zr_{50}Cu_{40}Al_{10}$ and $(Zr_{50}Cu_{40}Al_{10})_{98}Dy_2$ metallic glasses is 0.49 and 0.48, respectively,
 494 which indicates a slight increase of dynamic heterogeneity by introducing the element
 495 Dy. **Fig.12 (b)** displays the master curves fitted by **Eq.(9)** in the QPD model. The
 496 correlation factor χ values of $Zr_{50}Cu_{40}Al_{10}$ and $(Zr_{50}Cu_{40}Al_{10})_{98}Dy_2$ metallic glasses
 497 is 0.334 and 0.381, respectively. The results demonstrated that the increase of
 498 dynamic heterogeneity induced by introducing the Dy element, which is in good
 499 accordance with the discussion in the previous section.

500 The shift factor a_T versus various isothermal temperature for
 501 $(Zr_{50}Cu_{40}Al_{10})_{98}Dy_2$ metallic glasses is presented in **Fig.13**. According to the **Eq.(17)**,
 502 the apparent activation of α relaxation can be obtained. When the temperature
 503 increases, the viscosity increases sharply in the glass system, and the activation
 504 energy E_α is 6.08 and 5.96 eV for $Zr_{50}Cu_{40}Al_{10}$ and $(Zr_{50}Cu_{40}Al_{10})_{98}Dy_2$, respectively.

505 Noted that the activation energy E_α calculated here are nearly equal to the values
506 obtained in the previous section, this indicates that the activation energy of α
507 relaxation is an intrincically properties which does not change with the testing driven
508 frequency.

509 As we mentioned in the previous section, the correlation factor χ can be
510 determined by a plot of $\ln(\tan \delta)$ *versus* $\ln(\omega)$. As shown in **Fig.14**, all the
511 experimental results could be well described by the QPD model. It should be
512 mentioned that the correlation factor χ remains constant below the glass transition
513 temperature T_g , which is consistently with the prediction of QPD model. Based on
514 the QPD model, the microstructure of the glass materials is staying in an
515 iso-configuration state when the temperature below T_g . It implied that the
516 concentration of the “defects” concentration of glassy materials is nearly constant.
517 When the temperature surpasses the glass transition temperature T_g , the glassy
518 materials are no longer stay in an iso-configuration state. Consequently, the
519 correlation factor χ increases as a function of temperature. By increasing the
520 temperature, the atomic diffusion is accelerated in the case of metallic glasses or
521 molecules. It is expected that the correlation factor χ provides an indicator of
522 short-range order as well as the concentration of the quasi-point defects, which
523 reflects the atomic or molecular mobility in glassy solids [18, 25, 33].

524 Specifically, it is interesting to note that the parameter a in the **Eq.(6-3)**, which
525 indicates the slope of the curve $\ln(\tau)$ *versus* $1/T$ just above the glass transition
526 temperature T_g and the fragility parameter m for the metallic glass system but is
527 independent of the experimental condition (in opposition to the parameter m) [67,
528 81]. It can be seen that the value of the parameter a is $3.1 \times 10^{-3} \text{ K}^{-1}$ and $3.8 \times$
529 10^{-3} K^{-1} for $\text{Zr}_{50}\text{Cu}_{40}\text{Al}_{10}$ and $(\text{Zr}_{50}\text{Cu}_{40}\text{Al}_{10})_{98}\text{Dy}_2$ metallic glasses, respectively.
530 Based on the linear fit of the correlation factor χ with the temperature above the T_g
531 shown in **Fig.15**. The comparison between the prediction and experimental results of
532 various glass forming systems is summarized in **Table 2**. It can be seen that the value
533 of a of ZrCu-based metallic glass is intermediate between the reported oxidy glasses
534 and polymers. Thus, it demonstrates that the fragility for ZrCu-based metallic glass is

535 intermediate, meanwhile, close to the fragility of strong network glasses. It is in a good
 536 agreement with the fragility parameter m as mentioned in the previous section and
 537 the parameter a . As a consequence, the physical model could be used to succesfully
 538 describe the internal friction around the glass transition temperature in metallic
 539 glasses.

540 **Table 2** Parameters of the typical glassy materials used in the physical model [67]

Type	Material	T_g (K)	U_β (eV)	$\chi(T_g)$	a ($\times 10^{-3}$ K $^{-1}$)	Reference
Oxide	Silica	1493	-	0.47	-	[67]
	Silica-soda-lime	810	2.04	0.37	1	[67]
Metallic	Zr ₅₀ Cu ₄₀ Al ₁₀	691	0.628	0.383	3.1	Current work
	(Zr ₅₀ Cu ₄₀ Al ₁₀) ₉₈ Dy ₂	683	0.578	0.395	3.8	Current work
Polymeric	DGEBA-IPD	436	0.52	0.17	5.6	[67]
	PEEK	416	0.43/0.8	0.32	-	[67]
	PET	340	0.54	0.31	10	[67]
	PMABu	303	0.74	0.18	5	[67]
Molecular	Maltitol	310	0.61	0.34	5.3	[67]
	Sorbitol	268	0.61	0.32	5.8	[67]

541 3.2.3 Magnitude of the various components of the deformation

542 During the mechanical spectroscopy experiments of metallic glasses, three
 543 different components are involved in the mechanical response, i.e. elastic, viscoelastic
 544 and viscoplastic. With the set of constitutive equations recalled above, the QPD model
 545 allows a global description of the mechanical behaviour of an metallic glass from the
 546 linear to the non-linear range with account for the temperature, the loading conditions
 547 and the strain rate [53, 82]. Practically, this makes a strong correlations between the
 548 viscoelastic behavior of the metallic glass characterized by the dynamic mechanical
 549 analysis. Rinaldi et al. gave the expression of the general compliance [53]:

$$\begin{aligned}
 550 \quad J(t) = & J_{el} + \Delta J_\beta \sum_i W_\beta^i \left(1 - e^{(-t/\tau_\beta^i)}\right) + \Delta J_{ve} \sum_i W_{el}^i \left(1 - e^{(-t/\tau_\beta^i)}\right) + \\
 551 \quad & \Delta J_{vp} \sum_i W_{vp}^i \left(1 - e^{(-t/\tau_\beta^i)}\right) \quad (18)
 \end{aligned}$$

552 where J_{el} is the initial elastic compliance, taken as the inverse of the unrelaxed shear

553 modulus, W_{β}^i , W_{el}^i and W_{vp}^i are the relative weights of the Gumbel distribution law
 554 of the times τ_{β}^i , τ_{el}^i and τ_{vp}^i , respectively. Laplace-Carson transform of Eq.(18)
 555 directly gives the expression of the equivalent frequencial compliance J^* of the
 556 MGs:

$$557 \quad J^*(\omega) = J_{el} + J_{\beta} \sum_i \frac{W_{\beta}^i}{1+i\omega\tau_{\beta}^i} + J_{ve} \sum_i \frac{W_{ve}^i}{1+i\omega\tau_{ve}^i} + J_{vp} \sum_i \frac{W_{vp}^i}{1+i\omega\tau_{vp}^i} \quad (19)$$

558 The real part of J^* is noted J' and the imaginary part J'' . According to the
 559 previous research of Pelletier, the compliance can be deduced from the storage
 560 modulus and loss modulus (G' and G''): $J^* = J' - J'' = 1/G^* = 1/(G' + iG'') =$
 561 $J_{el} + J_{ve} + J_{vp}$ [22]. The imaginary parts is $J'' = -(J_{ve} + J_{vp})$.

562 **Fig.16 (a)** displays the evolution of J'' with the frequency. Both the low and
 563 high frequency sides tend toward a linear dependence with a slope of -0.8 and -1/3,
 564 respectively. Assuming a Newtonian flow, $J_{vp} = 1/\omega\eta$, the shear viscosity η can be
 565 expressed by: $\eta = G_u\tau_{mol}$, where G_u the unrelaxed is about 24 GPa. As shown in
 566 **Fig.12**, the characteristic time at T_g is $\tau_{mol} = 70$ s, so the shear viscosity η at this
 567 temperature is about 1.68×10^{12} Pa s. This is a reasonable value for the viscosity at
 568 T_g of metallic glasses. At the lower frequency, the visco-plasticity dominates the
 569 deformation process, this is because there is enough time for the atomic movements.
 570 By increasing of the frequency, visco-plasticity can not occur and the visco-elasticity
 571 becomes dominant. As proposed in a previous investigation [68], the elastic,
 572 visco-plastic and visco-plastic components over the whole frequency domain can be
 573 calculated as:

$$574 \quad J_{el} = J' = \frac{G'}{G'^2 + G''^2} \quad (20-1)$$

$$575 \quad J_{vp} = \frac{1}{\omega\eta} \quad (20-2)$$

$$576 \quad J_{ve} = J'' - J_{vp} \quad (20-3)$$

577 The contribution of the elasticity, viscoelasticity and viscoplasticity during the
 578 deformation process of $Zr_{50}Cu_{40}Al_{10}$ metallic glass were shown in **Fig.16 (b)**. As
 579 discussed above, the viscous flow is the main contribution at lower frequency domain,

580 while the viscoelasticity dominate the deformation behavior at the higher frequency.

581 **4. Conclusions**

582 In conclusion, the dynamic mechanical relaxation behavior of $Zr_{50}Cu_{40}Al_{10}$ and
583 $(Zr_{50}Cu_{40}Al_{10})_{98}Dy_2$ metallic glasses were investigated by DMA. Experimental results
584 demonstrated that micro-alloying plays an important role in the dynamic mechanical
585 behavior of the model alloys. Atomic mobility (i.e. concentration of the “quasi-point
586 defects”) increases by increasing the concent of Dy of $(Zr_{50}Cu_{40}Al_{10})_{100-x}Dy_x$ ($x=0$ or
587 2) glassy system. The quasi-point defects theory was used to describe the atomic
588 mobility and dynamic mechanical behavior of the $(Zr_{50}Cu_{40}Al_{10})_{100-x}Dy_x$ ($x=0$ or 2)
589 metallic glasses. The elastic, viscoelastic and viscoplastic response of the model alloy
590 was analyzed based on the deformation process. The correlation parameter χ can be
591 used to describe the concentration of the quasi-point defects, which is closely related
592 to the microstructural heterogeneity of glassy solids. The experimental results of the
593 ZrCu-based metallic glasses can be well described by the QPD theory. More
594 importantly, our findings based on the dynamic mechanical behavior provides a route
595 to understand the microstructural heterogeneity and physical properties of metallic
596 glasses.

597 **Acknowledgements**

598 This work is supported by the National Natural Science Foundation of China
599 (NSFC) (Grant Nos. 51971178 and 52171164), Natural Science Basic Research Plan
600 for Distinguished Young Scholars in Shaanxi Province (Grant No. 2021JC-12) and the
601 Natural Science Foundation of Chongqing (Grant No. cstc2020jcyj-jqX0001). The
602 authors would like to thank H. Chen (Yanshan University) for providing the help of
603 DSC experiments.

604

605 **References:**

- 606 [1] L.C. Zhang, Z. Jia, F. Lyu, S.X. Liang, J. Lu, A review of catalytic performance of
607 metallic glasses in wastewater treatment: Recent progress and prospects, *Prog. Mater.*
608 *Sci.* 105 (2019) 100576.
- 609 [2] J. Ding, S. Patinet, M.L. Falk, Y.Q. Cheng, E. Ma, Soft spots and their structural
610 signature in a metallic glass, *Proc. Natl. Acad. Sci. U.S.A.* 111(39) (2014)
611 14052-14056.
- 612 [3] N. Li, J.J. Zhang, W. Xing, D. Ouyang, L. Liu, 3D printing of Fe-based bulk
613 metallic glass composites with combined high strength and fracture toughness,
614 *Materials Design* 143 (2018) 285-296.
- 615 [4] K. Tao, J.C. Qiao, Q.F. He, K.K. Song, Y. Yang, Revealing the structural
616 heterogeneity of metallic glass: Mechanical spectroscopy and nanoindentation
617 experiments, *Int. J. Mech. Sci.* 201 (2021) 106469.
- 618 [5] W.H. Wang, The elastic properties, elastic models and elastic perspectives of
619 metallic glasses, *Prog. Mater. Sci.* 57(3) (2012) 487-656.
- 620 [6] X.Y. Wang, W.L. Dai, M. Zhang, P. Gong, N. Li, Thermoplastic micro-formability
621 of TiZrHfNiCuBe high entropy metallic glass, *J. Mater. Sci. Technol* 34(11) (2018)
622 2006-2013.
- 623 [7] L. Ward, S.C. O'Keeffe, J. Stevick, G.R. Jelbert, M. Aykol, C. Wolverton, A
624 machine learning approach for engineering bulk metallic glass alloys, *Acta Metall.*
625 159 (2018) 102-111.
- 626 [8] C.C. Yuan, F. Yang, X.K. Xi, C.L. Shi, D. Holland-Moritz, M.Z. Li, F. Hu, B.L.
627 Shen, X.L. Wang, A. Meyer, Impact of hybridization on metallic-glass formation and
628 design, *Mater. Today* 32 (2020) 26-34.
- 629 [9] M. Gao, J.H. Perepezko, Separating β relaxation from α relaxation in fragile
630 metallic glasses based on ultrafast flash differential scanning calorimetry, *Phys. Rev.*
631 *Mater.* 4(2) (2020) 025602.
- 632 [10] J.S. Harmon, M.D. Demetriou, W.L. Johnson, K. Samwer, Anelastic to plastic
633 transition in metallic glass-forming liquids, *Phys. Rev. Lett.* 99(13) (2007) 135502.
- 634 [11] J.D. Ju, M. Atzmon, A comprehensive atomistic analysis of the experimental

635 dynamic-mechanical response of a metallic glass, *Acta Metall.* 74 (2014) 183-188.

636 [12] J.C. Qiao, Q. Wang, J. Pelletier, H. Kato, R. Casalini, D. Crespo, E. Pineda, Y.

637 Yao, Y. Yang, Structural heterogeneities and mechanical behavior of amorphous alloys,

638 *Prog. Mater. Sci.* 104 (2019) 250-329.

639 [13] W.H. Wang, Dynamic relaxations and relaxation-property relationships in

640 metallic glasses, *Prog. Mater. Sci.* 106 (2019) 100561.

641 [14] A. Furukawa, H. Tanaka, Inhomogeneous flow and fracture of glassy materials,

642 *Nat. Mater.* 8(7) (2009) 601-609.

643 [15] Z. Lu, W. Jiao, W.H. Wang, H.Y. Bai, Flow unit perspective on room temperature

644 homogeneous plastic deformation in metallic glasses, *Phys. Rev. Lett.* 113(4) (2014)

645 045501.

646 [16] W. Peter G, Spatiotemporal structures in aging and rejuvenating glasses, *Proc.*

647 *Natl. Acad. Sci. U.S.A.* 106(5) (2009) 1353-1358.

648 [17] Y.Q. Cheng, E. Ma, H.W. Sheng, Atomic level structure in multicomponent bulk

649 metallic glass, *Phys. Rev. Lett.* 102(24) (2009) 245501.

650 [18] Y.H. Liu, T. Fujita, D. Aji, M. Matsuura, M.W. Chen, Structural origins of

651 Johari-Goldstein relaxation in a metallic glass, *Nat. Commun.* 5(1) (2014) 1-7.

652 [19] Y.H. Liu, D. Wang, K. Nakajima, W. Zhang, A. Hirata, T. Nishi, A. Inoue, M.W.

653 Chen, Characterization of nanoscale mechanical heterogeneity in a metallic glass by

654 dynamic force microscopy, *Phys. Rev. Lett.* 106(12) (2011) 125504.

655 [20] Q. Wang, J.J. Liu, Y.F. Ye, T.T. Liu, S. Wang, C.T. Liu, J. Lu, Y. Yang, Universal

656 secondary relaxation and unusual brittle-to-ductile transition in metallic glasses, *Mater.*

657 *Today* 20(6) (2017) 293-300.

658 [21] Z. Wang, W.H. Wang, Flow units as dynamic defects in metallic glassy materials,

659 *NATL SCI REV* 6(2) (2019) 304-323.

660 [22] J.M. Pelletier, V.d. Moortèle, Mechanical properties of bulk metallic glasses:

661 Elastic, visco-elastic and visco-plastic components in the deformation, *J. Non-Cryst.*

662 *Solids* 353(32-40) (2007) 3750-3753.

663 [23] J.C. Qiao, J.M. Pelletier, Dynamic mechanical relaxation in bulk metallic glasses:

664 a review, *J. Mater. Sci. Technol* 30(6) (2014) 523-545.

665 [24] J.C. Qiao, J.M. Pelletier, C. Esnouf, Y. Liu, H. Kato, Impact of the structural state
666 on the mechanical properties in a Zr–Co–Al bulk metallic glass, *J. Alloy Compd.* 607
667 (2014) 139-149.

668 [25] J.C. Qiao, Y. Yao, J.M. Pelletier, L.M. Keer, Understanding of micro-alloying on
669 plasticity in $\text{Cu}_{46}\text{Zr}_{47-x}\text{Al}_7\text{Dy}_x$ ($0 \leq x \leq 8$) bulk metallic glasses under compression:
670 based on mechanical relaxations and theoretical analysis, *Int. J. Plast.* 82 (2016)
671 62-75.

672 [26] L.T. Zhang, Y.J. Duan, D. Crespo, E. Pineda, Y.J. Wang, J.M. Pelletier, J.C. Qiao,
673 Dynamic mechanical relaxation and thermal creep of highentropy
674 $\text{La}_{30}\text{Ce}_{30}\text{Ni}_{10}\text{Al}_{20}\text{Co}_{10}$ bulk metallic glass, *Sci. China-Phys. Mech. Astron.* 64 (2021)
675 296111.

676 [27] G.P. Johari, M. Goldstein, Viscous liquids and the glass transition. II. Secondary
677 relaxations in glasses of rigid molecules, *J. Chem. Phys* 53(6) (1970) 2372-2388.

678 [28] X. Monnier, D. Cangialosi, B. Ruta, R. Busch, I. Gallino, Vitrification
679 decoupling from α -relaxation in a metallic glass, *Sci. Adv.* 6(17) (2020) 1454.

680 [29] H.B. Yu, W.H. Wang, K. Samwer, The β relaxation in metallic glasses: an
681 overview, *Mater. Today* 16(5) (2013) 183-191.

682 [30] F. Zhu, S.X. Song, K.M. Reddy, A. Hirata, M.W. Chen, Spatial heterogeneity as
683 the structure feature for structure–property relationship of metallic glasses, *Nat.*
684 *Commun.* 9(1) (2018) 1-7.

685 [31] P.G. Debenedetti, F.H. Stillinger, Supercooled liquids and the glass transition,
686 *Nature (London)* 410(6825) (2001) 259-267.

687 [32] A.S. Argon, Plastic deformation in metallic glasses, *Acta Metall.* 27(1) (1979)
688 47-58.

689 [33] S.G. Mayr, Activation energy of shear transformation zones: A key for
690 understanding rheology of glasses and liquids, *Phys. Rev. Lett.* 97(19) (2006) 195501.

691 [34] H.B. Yu, W.H. Wang, H.Y. Bai, Y. Wu, M.W. Chen, Relating activation of shear
692 transformation zones to β relaxations in metallic glasses, *Phys. Rev. B* 81(22) (2010)
693 220201.

694 [35] W.L. Johnson, K. Samwer, A universal criterion for plastic yielding of metallic

695 glasses with a $(T/T_g)^{2/3}$ temperature dependence, *Phys. Rev. Lett.* 95(19) (2005)
696 195501.

697 [36] Y.Q. Cheng, A.J. Cao, H.W. Sheng, E. Ma, Local order influences initiation of
698 plastic flow in metallic glass: Effects of alloy composition and sample cooling history,
699 *Acta Metall.* 56(18) (2008) 5263-5275.

700 [37] D. Granata, E. Fischer, J.F. Löffler, Effectiveness of hydrogen microalloying in
701 bulk metallic glass design, *Acta Metall.* 99 (2015) 415-421.

702 [38] L.S. Luo, B.B. Wang, F.Y. Dong, Y.Q. Su, E.Y. Guo, Y.J. Xu, M.Y. Wang, L.
703 Wang, J.X. Yu, R. Ritchie, Structural origins for the generation of strength, ductility
704 and toughness in bulk-metallic glasses using hydrogen microalloying, *Acta Metall.*
705 171 (2019) 216-230.

706 [39] N. Nollmann, I. Binkowski, V. Schmidt, H. Rösner, G. Wilde, Impact of
707 micro-alloying on the plasticity of Pd-based bulk metallic glasses, *Scr. Mater.* 111
708 (2016) 119-122.

709 [40] H.B. Yu, K. Samwer, W.H. Wang, H.Y. Bai, Chemical influence on β -relaxations
710 and the formation of molecule-like metallic glasses, *Nat. Commun.* 4(1) (2013) 1-6.

711 [41] B. Sarac, Y.P. Ivanov, A. Chuvilin, T. Schöberl, M. Stoica, Z.L. Zhang, J. Eckert,
712 Origin of large plasticity and multiscale effects in iron-based metallic glasses, *Nat.*
713 *Commun.* 9(1) (2018) 1-10.

714 [42] D. Şopu, S. Scudino, X.L. Bian, C. Gammer, J. Eckert, Atomic-scale origin of
715 shear band multiplication in heterogeneous metallic glasses, *Scr. Mater.* 178 (2020)
716 57-61.

717 [43] M. Bletry, P. Guyot, J.-J. Blandin, J.-L. Soubeyroux, Free volume model:
718 High-temperature deformation of a Zr-based bulk metallic glass, *Acta Metall.* 54(5)
719 (2006) 1257-1263.

720 [44] M.H. Cohen, D. Turnbull, Molecular transport in liquids and glasses, *J. Chem.*
721 *Phys* 31(5) (1959) 1164-1169.

722 [45] F. Spaepen, A microscopic mechanism for steady state inhomogeneous flow in
723 metallic glasses, *Acta Metallurgica* 25(4) (1977) 407-415.

724 [46] W. Jiao, P. Wen, H. Peng, H.Y. Bai, B.A. Sun, W.H. Wang, Evolution of

725 structural and dynamic heterogeneities and activation energy distribution of
726 deformation units in metallic glass, *Appl. Phys. Lett.* 102(10) (2013) 101903.

727 [47] Z. Wang, B.A. Sun, H.Y. Bai, W.H. Wang, Evolution of hidden localized flow
728 during glass-to-liquid transition in metallic glass, *Nat. Commun.* 5 (2014) 5823.

729 [48] A. Granato, Interstitialcy model for condensed matter states of
730 face-centered-cubic metals, *Phys. Rev. Lett.* 68(7) (1992) 974.

731 [49] A.V. Granato, Interstitialcy theory of simple condensed matter, *EUR. PHYS. J. B*
732 87(1) (2014) 1-6.

733 [50] D.N. Perera, A.P. Tsai, Dynamic tensile measurements for below the calorimetric
734 glass transition temperature, *Journal of Physics: Condensed Matter* 11(15) (1999)
735 3029.

736 [51] J. Perez, Quasi-punctual defects in vitreous solids and liquid-glass transition,
737 *Solid State Ionics* 39(1) (1990) 69-79.

738 [52] J. Perez, J.Y. Cavaille, Temperature dependence of the molecular dynamics in
739 amorphous polymers through the rubber-glass transition, *J. Non-Cryst. Solids* 172
740 (1994) 1028-1036.

741 [53] R. Rinaldi, R. Gaertner, L. Chazeau, C. Gauthier, Modelling of the mechanical
742 behaviour of amorphous glassy polymer based on the Quasi Point Defect
743 theory—Part I: Uniaxial validation on polycarbonate, *Int. J. Nonlin. Mech.* 46(3)
744 (2011) 496-506.

745 [54] J.M. Pelletier, J. Perez, L. Duffrene, Mechanical response of an oxide glass to
746 mechanical loading—shear and volume relaxation effects: physical analysis, *Acta*
747 *Metall.* 48(6) (2000) 1397-1408.

748 [55] S. Etienne, J.Y. Cavallé, J. Perez, R. Point, M. Salvia, Automatic system for
749 analysis of micromechanical properties, *Rev. Sci. Instrum.* 53(8) (1982) 1261-1266.

750 [56] Y.T. Cheng, Q. Hao, J.C. Qiao, D. Crespo, E. Pineda, J.M. Pelletier, Effect of
751 minor addition on dynamic mechanical relaxation in ZrCu-based metallic glasses, *J.*
752 *Non-Cryst. Solids* (2020) 120496.

753 [57] J.C. Qiao, Y.X. Chen, J.M. Pelletier, H. Kato, D. Crespo, Y. Yao, V.A. Khonik,
754 *Viscoelasticity of Cu-and La-based bulk metallic glasses: Interpretation based on the*

755 quasi-point defects theory, *Mater. Sci. Eng. A* 719 (2018) 164-170.

756 [58] Z.F. Zhao, P. Wen, C.H. Shek, W.H. Wang, Measurements of slow β -relaxations
757 in metallic glasses and supercooled liquids, *Phys. Rev. B* 75(17) (2007) 174201.

758 [59] C.A. Angell, Formation of glasses from liquids and biopolymers, *Science*
759 267(5206) (1995) 1924-1935.

760 [60] Z.F. Yao, J.C. Qiao, J.M. Pelletier, Y. Yao, Characterization and modeling of
761 dynamic relaxation of a Zr-based bulk metallic glass, *J. Alloy Compd.* 690 (2017)
762 212-220.

763 [61] A. Takeuchi, A. Inoue, Calculations of mixing enthalpy and mismatch entropy for
764 ternary amorphous alloys, *Mater. T. JIM* 41(11) (2000) 1372-1378.

765 [62] A. Takeuchi, A. Inoue, Classification of bulk metallic glasses by atomic size
766 difference, heat of mixing and period of constituent elements and its application to
767 characterization of the main alloying element, *Mater. Trans.* 46(12) (2005) 2817-2829.

768 [63] J.Y. Cavaille, J. Perez, G.P. Johari, Molecular theory for the rheology of glasses
769 and polymers, *Phys. Rev. B* 39(4) (1989) 2411.

770 [64] J.Y. Cavaille, J. Perez, G.P. Johari, A comparison of a point defects theory with
771 mechanical relaxations in polymers, *J. Non-Cryst. Solids* 131 (1991) 935-941.

772 [65] M.B.M. Mangion, J.Y. Cavaille, J. Perez, A molecular theory for the sub-T_g
773 plastic mechanical response of amorphous polymers, *Philos. Mag. A* 66(5) (1992)
774 773-796.

775 [66] R.G. Palmer, D.L. Stein, E. Abrahams, P.W. Anderson, Models of hierarchically
776 constrained dynamics for glassy relaxation, *Phys. Rev. Lett.* 53(10) (1984) 958.

777 [67] C. Gauthier, J.M. Pelletier, L. David, G. Vigier, J. Perez, Relaxation of
778 non-crystalline solids under mechanical stress, *J. Non-Cryst. Solids* 274(1-3) (2000)
779 181-187.

780 [68] J.M. Pelletier, B. Van de Moortèle, I. Lu, Viscoelasticity and viscosity of Pd–Ni–
781 Cu–P bulk metallic glasses, *Mater. Sci. Eng. A* 336(1-2) (2002) 190-195.

782 [69] Q. Wang, J.M. Pelletier, Y.D. Dong, Y.F. Ji, Structural relaxation and
783 crystallisation of bulk metallic glasses $Zr_{41}Ti_{14}Cu_{12.5}Ni_{10-x}Be_{22.5}Fe_x$ ($x= 0$ or 2)
784 studied by mechanical spectroscopy, *Mater. Sci. Eng. A* 370(1-2) (2004) 316-320.

785 [70] L.S. Huo, J.F. Zeng, W.H. Wang, C.T. Liu, Y. Yang, The dependence of shear
786 modulus on dynamic relaxation and evolution of local structural heterogeneity in a
787 metallic glass, *Acta Metall.* 61(12) (2013) 4329-4338.

788 [71] T.J. Lei, L.R. DaCosta, M. Liu, J. Shen, Y.H. Sun, W.H. Wang, M. Atzmon,
789 Composition dependence of metallic glass plasticity and its prediction from anelastic
790 relaxation—A shear transformation zone analysis, *Acta Metall.* 195 (2020) 81-86.

791 [72] H.B. Yu, X. Shen, Z. Wang, L. Gu, W.H. Wang, H.Y. Bai, Tensile plasticity in
792 metallic glasses with pronounced β relaxations, *Phys. Rev. Lett.* 108(1) (2012)
793 015504.

794 [73] A. Taub, F. Spaepen, The kinetics of structural relaxation of a metallic glass, *Acta*
795 *Metall.* 28(12) (1980) 1781-1788.

796 [74] S. Tsao, F. Spaepen, Structural relaxation of a metallic glass near equilibrium,
797 *Acta Metall.* 33(5) (1985) 881-889.

798 [75] J.C. Qiao, Y.J. Wang, J.M. Pelletier, L.M. Keer, M.E. Fine, Y. Yao,
799 Characteristics of stress relaxation kinetics of $\text{La}_{60}\text{Ni}_{15}\text{Al}_{25}$ bulk metallic glass, *Acta*
800 *Metall.* 98 (2015) 43-50.

801 [76] A. Slipenyuk, J. Eckert, Correlation between enthalpy change and free volume
802 reduction during structural relaxation of $\text{Zr}_{55}\text{Cu}_{30}\text{Al}_{10}\text{Ni}_5$ metallic glass, *Scr. Mater.*
803 50(1) (2004) 39-44.

804 [77] J.C. Qiao, R. Casalini, J.M. Pelletier, H. Kato, Characteristics of the structural
805 and Johari–Goldstein relaxations in Pd-based metallic glass-forming liquids, *J. Phys.*
806 *Chem. B* 118(13) (2014) 3720-3730.

807 [78] H.T. Jeong, J.M. Park, W.T. Kim, D.H. Kim, Quasicrystalline effects on the
808 mechanical relaxation behavior of a $\text{Ti}_{45}\text{Zr}_{16}\text{Ni}_9\text{Cu}_{10}\text{Be}_{20}$ metallic glass, *Mater. Sci.*
809 *Eng. A* 527(1-2) (2009) 1-6.

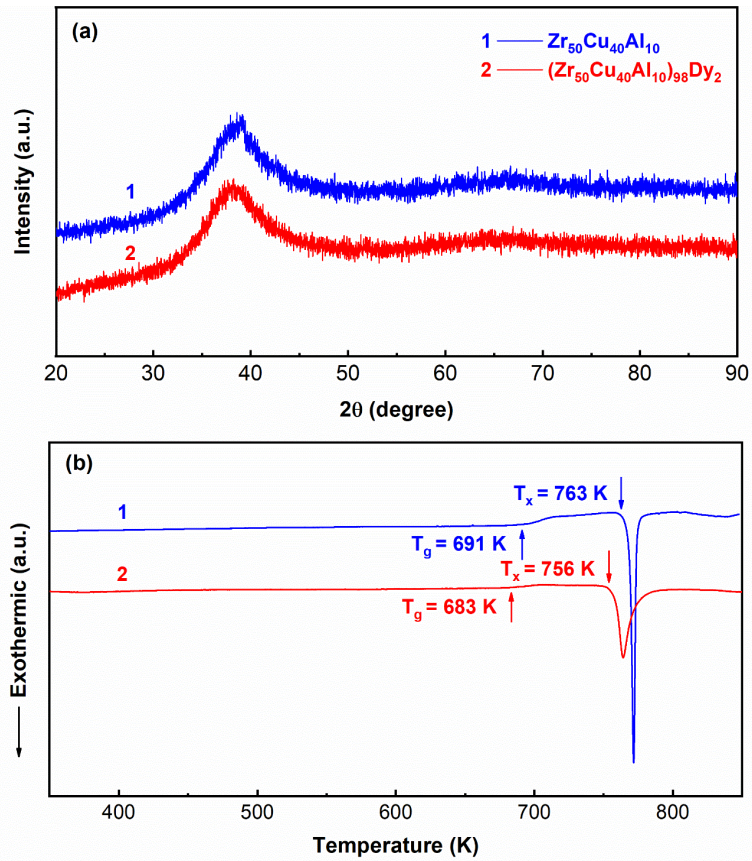
810 [79] G. Williams, D.C. Watts, Non-symmetrical dielectric relaxation behaviour arising
811 from a simple empirical decay function, *Trans. Faraday Society* 66 (1970) 80-85.

812 [80] R. Bergman, General susceptibility functions for relaxations in disordered
813 systems, *J. Appl. Phys.* 88(3) (2000) 1356-1365.

814 [81] Q. Wang, J.M. Pelletier, J. Lu, Y.D. Dong, Study of internal friction behavior in a

815 Zr base bulk amorphous alloy around the glass transition, Mater. Sci. Eng. A 403(1-2)
816 (2005) 328-333.
817 [82] N. Ouali, M. Mangion, J. Perez, Experimental and theoretical analysis of both the
818 small-and the large-stress mechanical response of poly (methyl methacrylate), Philos.
819 Mag. A 67(4) (1993) 827-848.
820

821 Captions of figures:

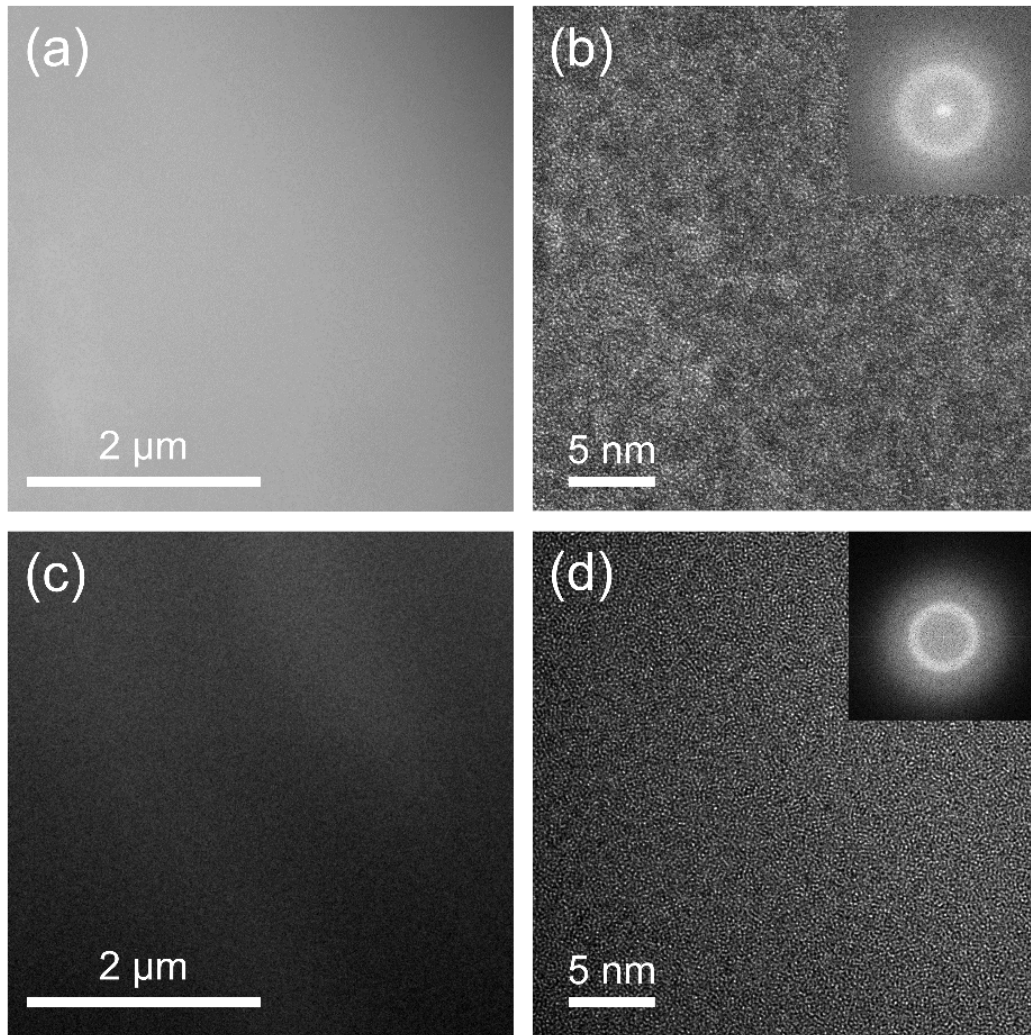


822

823 **Fig.1** (a) The typical XRD patterns and (b) DSC curves of $(Zr_{50}Cu_{40}Al_{10})_{100-x}Dy_x$ ($x=0$

824 or 2) bulk metallic glasses (heating rate is 10 K/min).

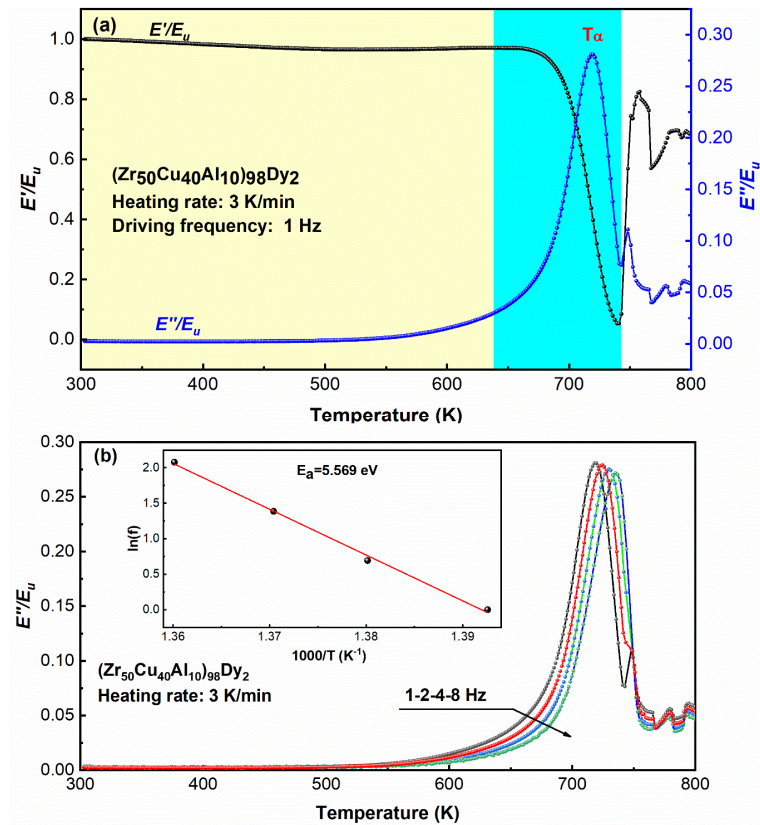
825



826

827 **Fig.2** (a) TEM micrograph and (b) HRTEM image of as-cast $Zr_{50}Cu_{40}Al_{10}$ metallic
828 glass. (c) TEM micrograph and (d) HRTEM image of $(Zr_{50}Cu_{40}Al_{10})_{98}Dy_2$ metallic
829 glass. Insets in (b) and (d) showing the corresponding FFT images.

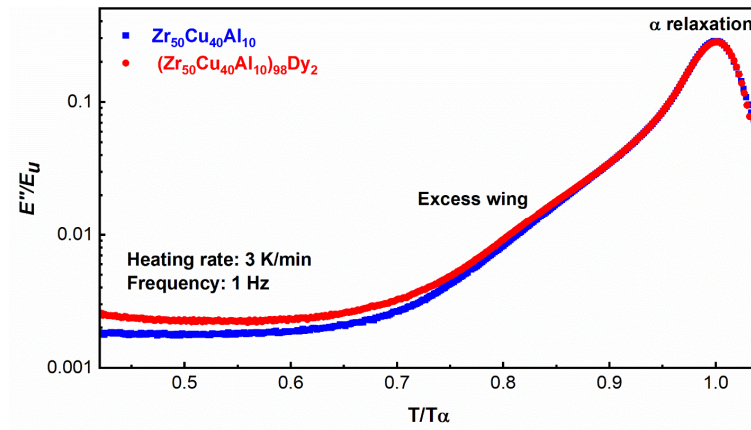
830



831

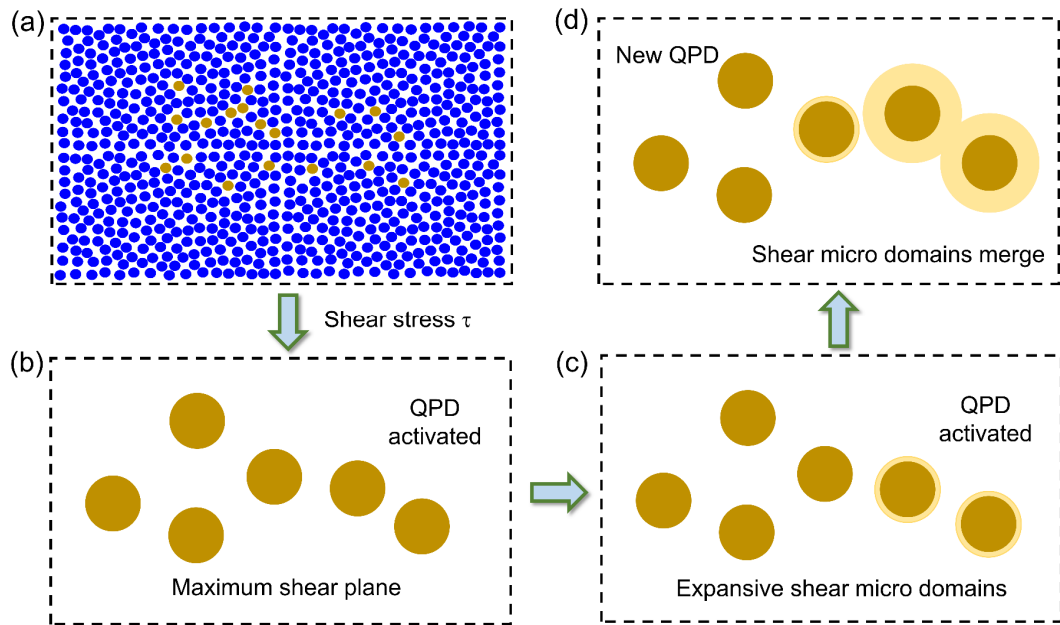
832 **Fig.3** (a) Normalized storage modulus and loss modulus of $(\text{Zr}_{50}\text{Cu}_{40}\text{Al}_{10})_{98}\text{Dy}_2$
 833 metallic glass as function of the temperature; (b) The normalized loss modulus as
 834 function of the temperature of $(\text{Zr}_{50}\text{Cu}_{40}\text{Al}_{10})_{98}\text{Dy}_2$ metallic glass with different
 835 driving frequency. Inset is the Arrhenius relation of peak frequency of loss modulus
 836 *versus* the reciprocal of temperature.)

837



838

839 **Fig.4** Temperature dependence of the normalized loss modulus E''/E_u in the
 840 $(\text{Zr}_{50}\text{Cu}_{40}\text{Al}_{10})_{100-x}\text{Dy}_x$ ($x=0$ or 2) metallic glasses.



841

842

843

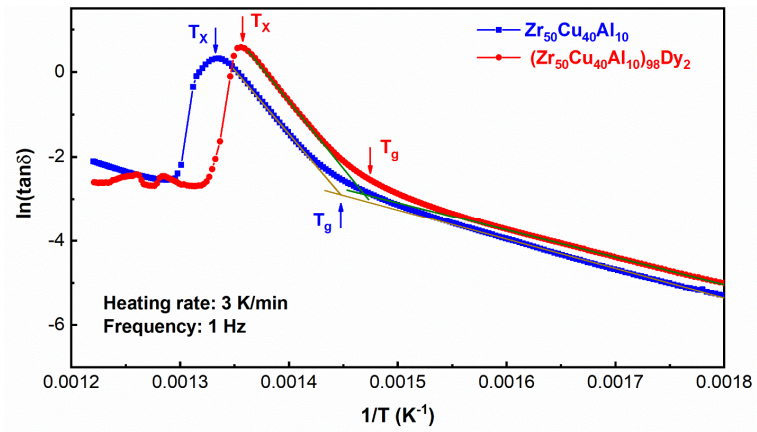
844

845

846

847

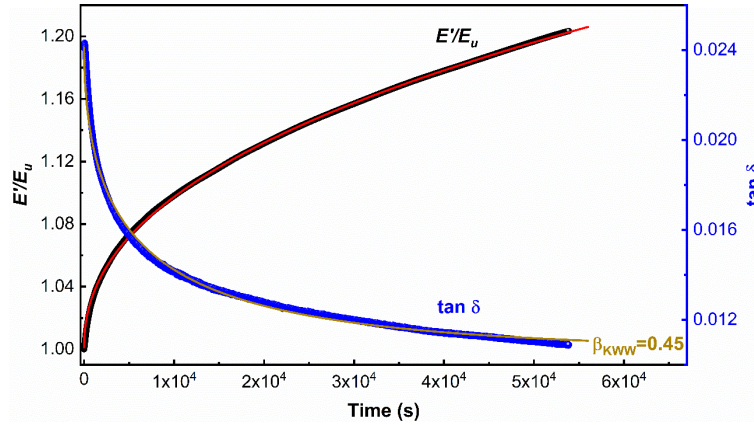
Fig.5 Conceptual description of the microstructural arrangements within a glassy amorphous material as posted by the QPD model: (a) original configuration of the glassy state, the golden and blue balls represent quasi point defects and elastic matrix, respectively, (b,c,d) micro structural reorganization (activation of these QPD and growth of sheared micro domains) provoked by an external thermomechanical stimuli.



848

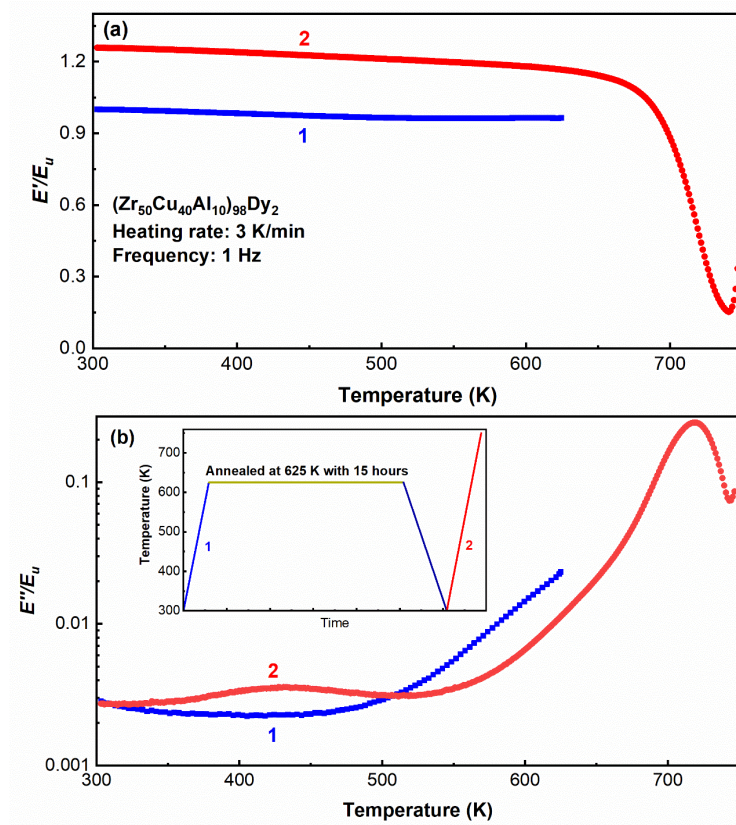
849 **Fig.6** Logarithm of the internal friction $\ln(\tan \delta)$ *versus* reciprocal of the
 850 temperature $1/T$ of the $(\text{Zr}_{50}\text{Cu}_{40}\text{Al}_{10})_{100-x}\text{Dy}_x$ ($x=0$ or 2) bulk metallic glasses.

851



852

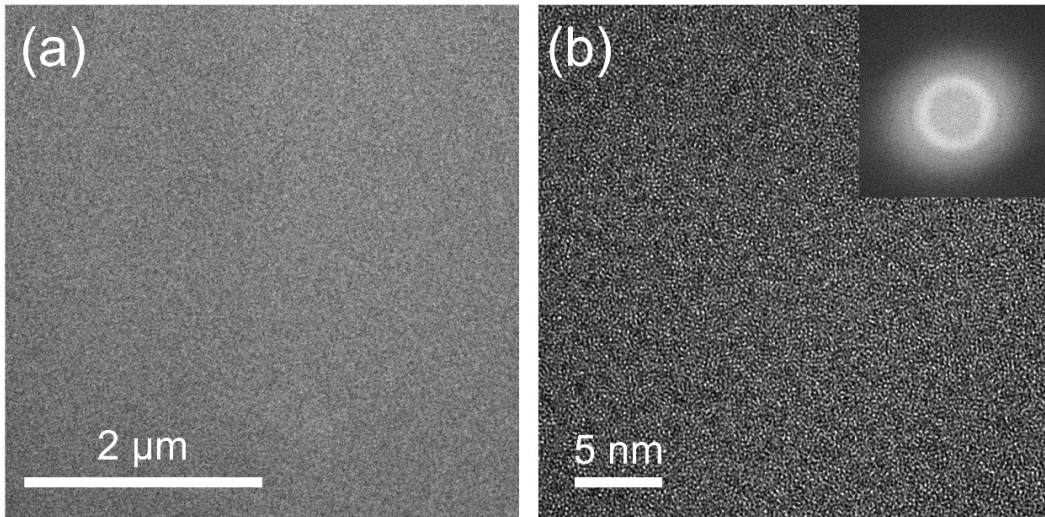
853 **Fig.7** Evolution of the storage modulus E'/E_u and the loss factor $\tan \delta$ with the
 854 aging time at 625 K in the $(Zr_{50}Cu_{40}Al_{10})_{98}Dy_2$ metallic glass. The solid lines are
 855 fitted by the KWW equation of the **Eq.(12)**.
 856



857

858 **Fig.8** Effect of the physical aging below the glass transition temperature on the
 859 dynamic mechanical behavior of the $(Zr_{50}Cu_{40}Al_{10})_{98}Dy_2$ metallic glass. (a)
 860 Normalized storage modulus of $(Zr_{50}Cu_{40}Al_{10})_{98}Dy_2$ metallic glass at as-cast state and
 861 annealed state. (b) Normalized loss modulus of $(Zr_{50}Cu_{40}Al_{10})_{98}Dy_2$ metallic glass at
 862 as-cast state and annealed state.

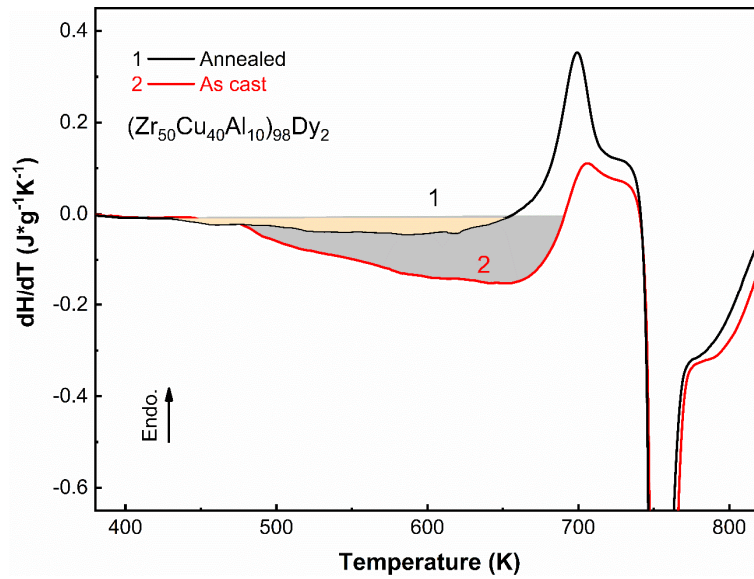
863



864

865 **Fig.9** (a) TEM micrograph and (b) HRTEM image of the annealed
866 $(\text{Zr}_{50}\text{Cu}_{40}\text{Al}_{10})_{98}\text{Dy}_2$ metallic glass with an inset in (b) showing the corresponding FFT
867 image.

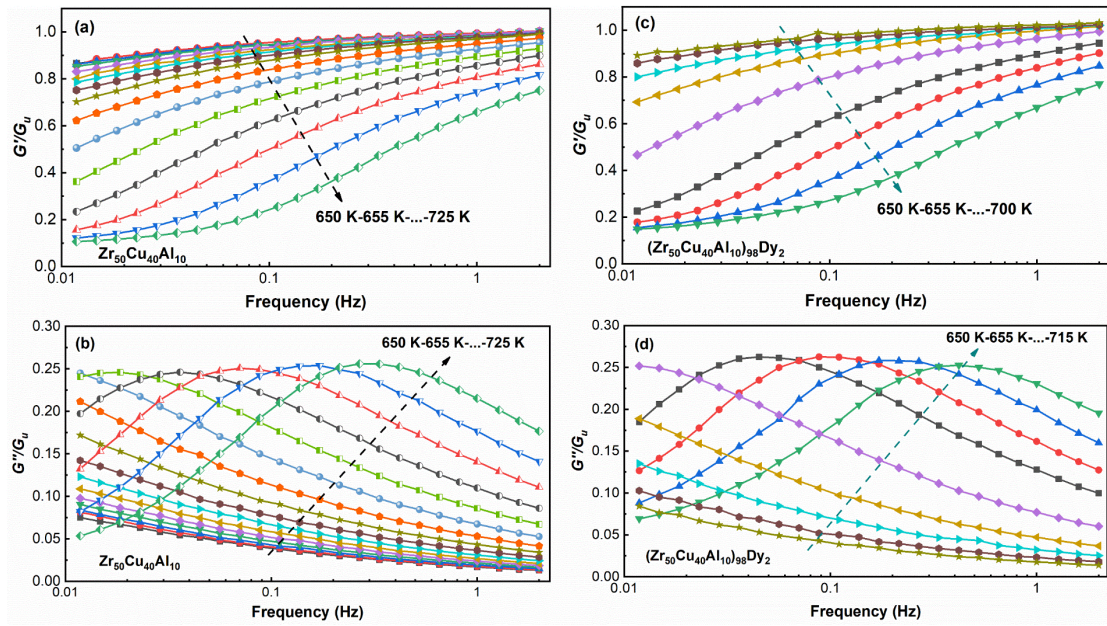
868



869

870 **Fig.10** Relaxation enthalpy from the differential scanning calorimetry traces of
 871 $(\text{Zr}_{50}\text{Cu}_{40}\text{Al}_{10})_{98}\text{Dy}_2$ bulk metallic glass: as-cast state and annealed sample (annealing
 872 temperature T_a is 625 K with annealing time is 15 h). The relaxation enthalpy (ΔH)
 873 gradually decreases after annealing below the glass transition temperature T_g .

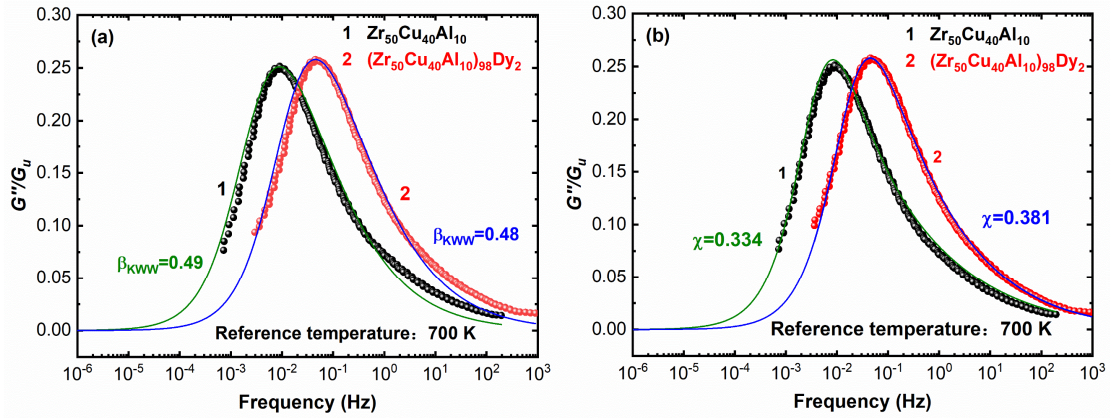
874



875

876 **Fig.11** Normalized shear modulus as a function of frequency at different temperature
 877 of $(\text{Zr}_{50}\text{Cu}_{40}\text{Al}_{10})_{100-x}\text{Dy}_x$ ($x=0$ or 2) bulk metallic glasses: (a) Storage modulus
 878 G'/G_u of $\text{Zr}_{50}\text{Cu}_{40}\text{Al}_{10}$ metallic glass and (b) Loss modulus G''/G_u of $\text{Zr}_{50}\text{Cu}_{40}\text{Al}_{10}$
 879 metallic glass, (c) Storage modulus G'/G_u of $(\text{Zr}_{50}\text{Cu}_{40}\text{Al}_{10})_{98}\text{Dy}_2$ metallic glass and
 880 (d) Loss modulus G''/G_u of $(\text{Zr}_{50}\text{Cu}_{40}\text{Al}_{10})_{98}\text{Dy}_2$ metallic glass.

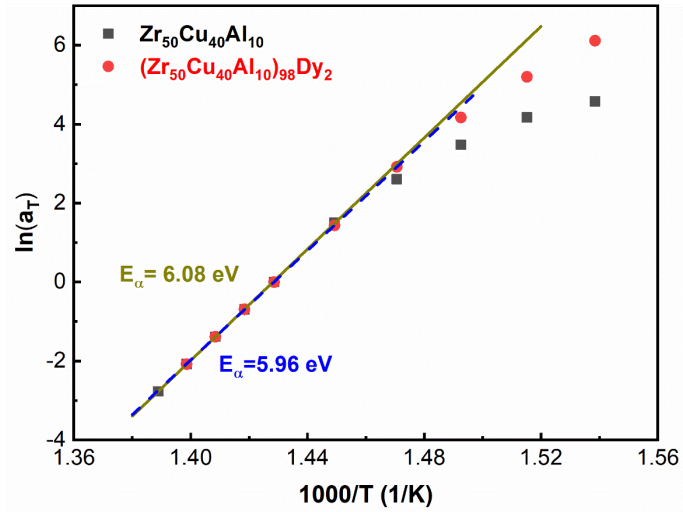
881



882

883 **Fig.12** The master curves of the normalized loss modulus G''/G_u of the
 884 $(Zr_{50}Cu_{40}Al_{10})_{100-x}Dy_x$ ($x=0$ or 2) bulk metallic glasses. The reference temperature is
 885 700 K. (a) The solid lines are fitted by the **Eq.(17)** of KWW equation; (b) The solid
 886 lines are fitted by the **Eq.(9)** of QPD theory.

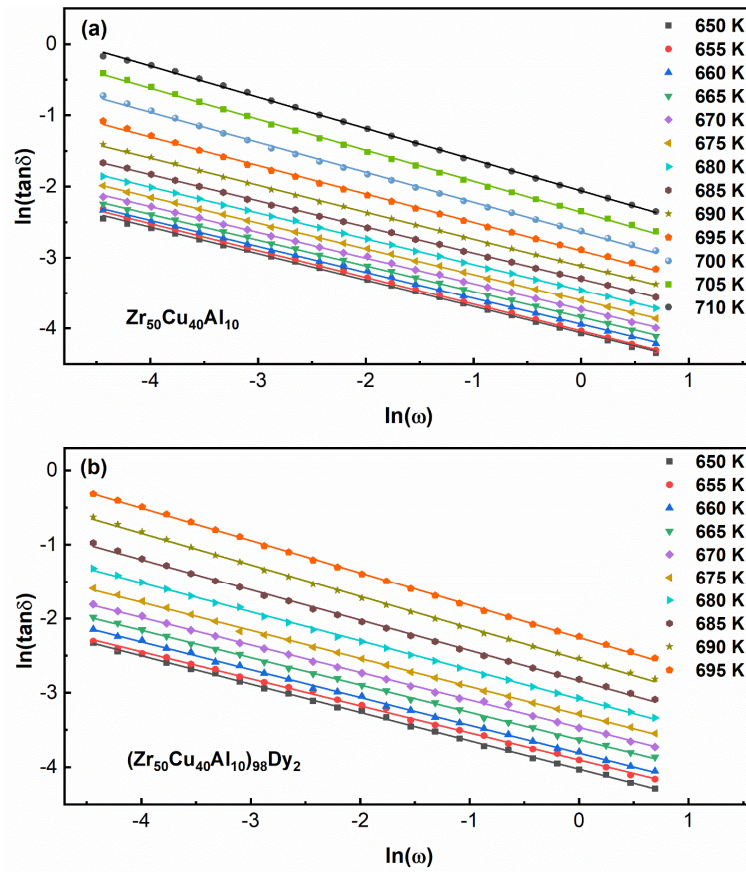
887



888

889 **Fig.13** Temperature dependence of the shift factor for the $(\text{Zr}_{50}\text{Cu}_{40}\text{Al}_{10})_{100-x}\text{Dy}_x$ ($x=0$
 890 or 2) bulk metallic glasses. The apparent activation energy E_α of the α relaxation
 891 process was marked in the figure (the fitting lines are the Arrhenius plots).

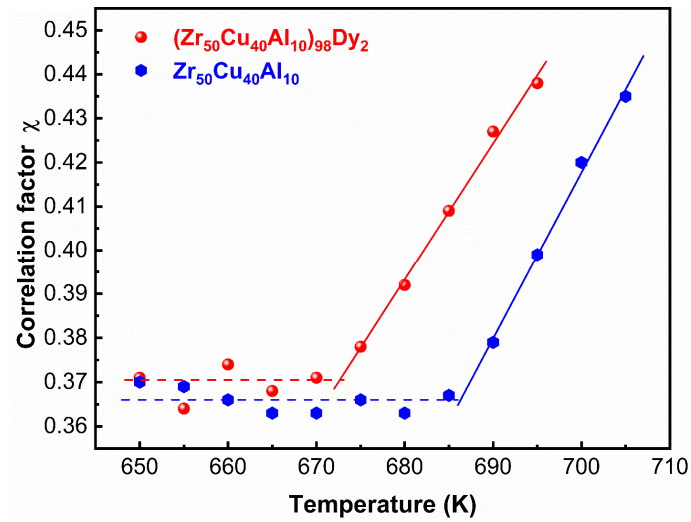
892



893

894 **Fig.14** Effect of the driving frequency on the loss factor $\tan \delta$ at various
 895 temperature of $\text{Zr}_{50}\text{Cu}_{40}\text{Al}_{10}$ metallic glass (a) and $(\text{Zr}_{50}\text{Cu}_{40}\text{Al}_{10})_{98}\text{Dy}_2$ metallic glass
 896 (b). Solid lines are fitted by the **Eq.(10)**.

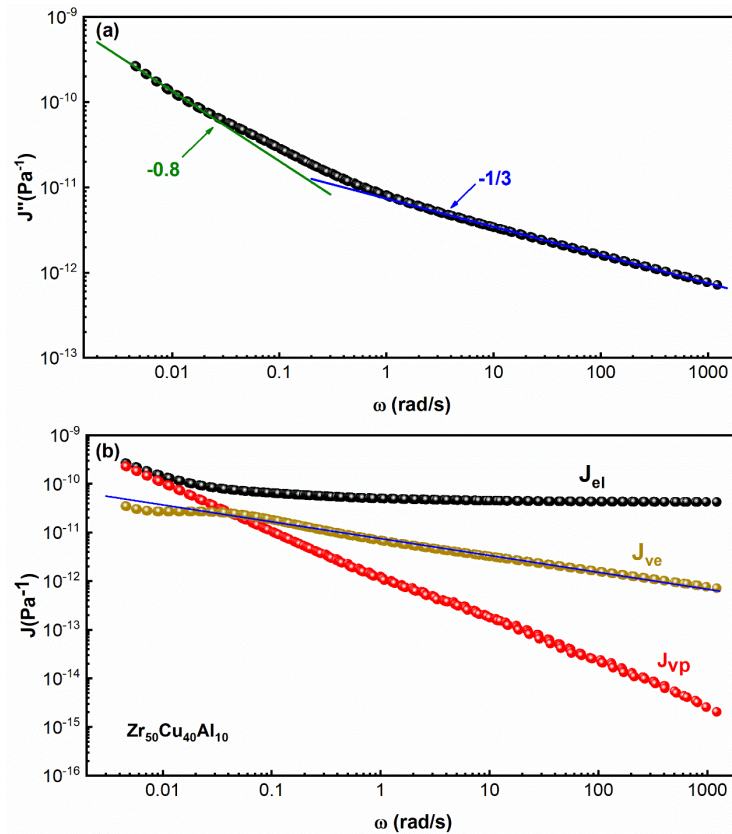
897



898

899 **Fig.15** The correlation factor χ as a function of temperature of the
 900 $(\text{Zr}_{50}\text{Cu}_{40}\text{Al}_{10})_{100-x}\text{Dy}_x$ ($x=0$ or 2) bulk metallic glasses.

901



902

903 **Fig.16** (a) Imaginary compliance *versus* the angular frequency of $Zr_{50}Cu_{40}Al_{10}$
 904 metallic glass; (b) Different components of the compliance J as a function of the
 905 angular frequency ω . The reference temperature is 700 K.

Graphical Abstract

